

CAST-CKT: Chaos-Aware Spatio-Temporal and Cross-City Knowledge Transfer for Traffic Flow Prediction

Abdul Joseph Fofanah¹, Lian Wen¹, David Chen¹, Alpha Alimamy Kamara², Zhongyi Zhang¹

¹School of Information and Communication Technology, Griffith University, Queensland, Australia

²School of Computer Science and Engineering, Central South University, Changsha, China

abdul.fofanah@griffithuni.edu.au, l.wen@griffith.edu.au, david.chen@griffith.edu.au,
kamara@csu.edu.cn, zhongyi.zhang@griffithuni.edu.au

Abstract

Traffic prediction in data-scarce, cross-city settings is challenging due to complex nonlinear dynamics and domain shifts. Existing methods often fail to capture traffic's inherent chaotic nature for effective few-shot learning. We propose CAST-CKT, a novel Chaos-Aware Spatio-Temporal and Cross-City Knowledge Transfer framework. It employs an efficient chaotic analyser to quantify traffic predictability regimes, driving several key innovations: chaos-aware attention for regime-adaptive temporal modelling; adaptive topology learning for dynamic spatial dependencies; and chaotic consistency-based cross-city alignment for knowledge transfer. The framework also provides horizon-specific predictions with uncertainty quantification. Theoretical analysis shows improved generalisation bounds. Extensive experiments on four benchmarks in cross-city few-shot settings show CAST-CKT outperforms state-of-the-art methods by significant margins in MAE and RMSE, while offering interpretable regime analysis. Code is available at <https://github.com/afofanah/CAST-CKT>.

1 Introduction

Traffic flow prediction has emerged as a critical component of intelligent transportation systems, with applications ranging from congestion management to autonomous vehicle navigation [Li *et al.*, 2017], [Wu *et al.*, 2020], [Wang *et al.*, 2025]. Despite significant advances in spatio-temporal graph neural networks, accurately forecasting traffic patterns remains particularly challenging in data-scarce scenarios and across diverse urban environments due to inherent nonlinear dynamics, chaotic behaviour, and complex dependencies in urban mobility systems [Zhang *et al.*, 2021] [Jiang *et al.*, 2023].

Current approaches face three fundamental limitations in few-shot cross-city scenarios. First, existing methods primarily rely on abundant historical data from individual urban environments [Huang *et al.*, 2019], [Jin *et al.*, 2022], assuming stationary patterns while neglecting intrinsic chaotic characteristics. Second, they lack effective mechanisms for cross-city knowledge transfer, struggling to generalise when histor-

ical data is limited due to new sensor deployments or emerging urban configurations, [Tang *et al.*, 2022]. Third, standard message-passing schemes cannot adapt to varying dynamical regimes across cities with limited training instances, [Tabatabaie *et al.*, 2025].

Chaos theory provides powerful theoretical tools for analysing complex dynamical systems that appear random but are governed by deterministic rules, [Odibat and Baleanu, 2022]. In traffic systems, chaos manifests through sensitive dependence on initial conditions, fractal patterns in congestion formation, and multiple attractors representing different traffic regimes [Fofanah *et al.*, 2025]. Key chaos indicators, such as Lyapunov exponents, fractal dimensions, and entropy measures, offer quantitative characterisations of system predictability and complexity [McAllister *et al.*, 2024]. However, current traffic prediction models largely ignore these chaos theory principles, missing opportunities for regime-adaptive forecasting that could significantly enhance the few-shot generalisation.

Based on the critical gaps we have identified in existing approaches, specifically the lack of chaos theory integration and the inability to adapt to dynamic regimes, we must confront the following two core challenges when constructing predictive models for data-scarce or novel urban environments [Hospedales *et al.*, 2021], [Qian *et al.*, 2023b], [Novak *et al.*, 2023]: **Challenge 1: How to integrate chaos-theoretic principles for adaptive regime switching in few-shot forecasting?** This involves developing mechanisms that can detect shifts in a system's dynamical regime (e.g., from laminar to chaotic flow) using minimal data and adjust model behaviour and uncertainty estimates accordingly, moving beyond static spatial or statistical alignment. **Challenge 2: How to design a cross-city, few-shot optimisation framework that explicitly accounts for intrinsic dynamical similarity?** This requires moving beyond topological feature alignment to instead identify and leverage shared nonlinear dynamical characteristics between cities, enabling rapid adaptation based on universal chaos metrics rather than extensive historical data. **Challenge 3: How do you ensure the computational tractability and real-time applicability of chaos-aware modelling in large-scale urban networks?** Extracting and integrating high-dimensional chaos features, such as Lyapunov exponents, fractal dimensions, and recurrence metrics, which imposes significant computational overhead. Scaling these operations

to city-wide sensor networks with thousands of nodes and high-frequency data streams, while meeting the latency requirements of real-time traffic management, remains an open practical hurdle.

To address these challenges, we propose Chaos-Aware Spatio-Temporal Cross-City Knowledge Transfer (CAST-CKT), a novel framework that integrates chaos theory, few-shot meta-learning, and cross-city transfer for robust traffic forecasting under data scarcity. The framework is realised through key technical innovations: an efficient chaos analyser that extracts a multifaceted feature vector to quantify predictability; a chaos-conditioned attention mechanism that adapts temporal modelling to the current dynamical regime; and an adaptive graph learner that constructs spatial relationships informed by both node features and chaotic characteristics. Operationally, CAST-CKT proceeds through three core phases: 1) In the *Chaos Analysis and Regime Characterisation Phase*, we compute nonlinear dynamics metrics from minimal data to quantitatively characterise the current traffic predictability regime. 2) In the *Adaptive Graph Learning and Conditioning Phase*, we construct a regime-aware graph structure that dynamically adjusts spatial relationship modelling based on the characterised dynamical state. 3) In the *Chaos-Aware Meta-Transfer Phase*, we employ a meta-learning protocol optimised for rapid adaptation by leveraging shared, transferable dynamical patterns across cities. Theoretically, to the best of our knowledge, we are the first to investigate the principled integration of chaos theory with spatio-temporal few-shot learning for traffic forecasting. Our primary contributions are fourfold:

- *A Chaos Theory Foundation for Transferable Predictability:* We propose the novel concept of a chaos profile as a complete dynamical signature for traffic systems and formally establish that matching these profiles between cities guarantees transferable predictability, creating the first theoretically grounded alignment metric for cross-city knowledge transfer.
- *The CAST-CKT Architecture for Regime-Aware Modelling:* We design CAST-CKT, the first end-to-end model that unifies chaos theory with spatio-temporal learning. It features a chaos-conditioned attention mechanism and adaptive graph learning, all dynamically modulated by quantitative chaos features to handle diverse, unseen predictability regimes in a holistic few-shot adaptation system.
- *Holistic Few-Shot Adaptation System:* We develop CAST-CKT into an extensive adaptation framework where a target city's chaos profile explicitly guides meta-learning optimisation and horizon-specific uncertainty quantification. This ensures rapid, regime-aware adaptation by incorporating chaos dynamics directly into the learning process, allowing the model to quickly adjust to new urban environments with minimal data.
- *Empirical Validation and Reliable Uncertainty Quantification:* We validate the framework on multiple real-world datasets under strict few-shot, cross-city settings. CAST-CKT consistently outperforms state-of-the-art baselines while providing interpretable regime

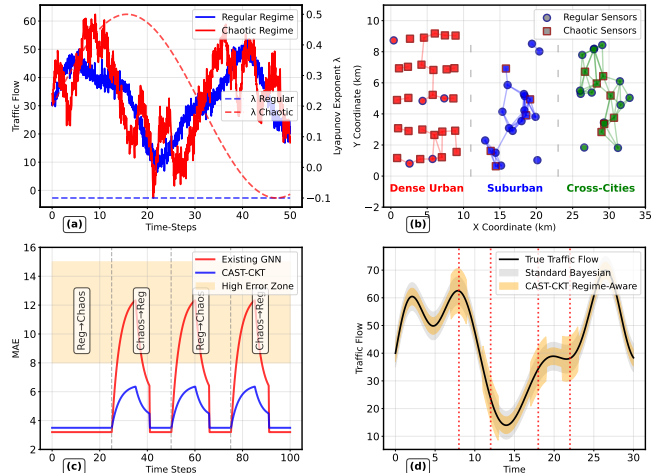


Figure 1: Motivation for chaos-informed cross-city forecasting. (a) Regular vs chaotic traffic regimes with different predictability horizons. (b) Heterogeneous multi-city sensor distributions. (c) Cross-regime transfer robustness of CAST-CKT vs existing GNNs. (d) Regime-aware vs uniform uncertainty estimates.

analysis and reliable, calibrated uncertainty estimates, confirming its effectiveness in data-scarce, dynamically shifting environments.

2 Motivation

Cross-city traffic forecasting under data scarcity remains highly challenging because traffic dynamics vary substantially across cities and regimes. Prior work has shown that traffic flow exhibits chaotic behaviour [Dendrinos, 1994; Zhao *et al.*, 2017; Shang *et al.*, 2005], yet this insight has not been fully exploited in modern learning-based forecasting systems. In particular, three critical gaps remain.

First, chaos measures such as Lyapunov exponents, entropy, and long-range dependence are typically used only for post hoc analysis rather than being integrated into predictive models [Zhou *et al.*, 2019; Anusree and Pramod, 2025]. Second, existing few-shot and cross-city transfer methods assume that cities are comparable based on spatial or statistical similarity, ignoring differences in their underlying dynamical regimes [Lu *et al.*, 2022a; Yao *et al.*, 2019]. Third, uncertainty estimation methods are largely regime-agnostic, producing overly uniform confidence intervals that fail to reflect rapid changes in predictability [Qian *et al.*, 2023a; Hu *et al.*, 2024].

Figure 1 illustrates these challenges. (a) shows that traffic can switch between regular and chaotic regimes with different predictability horizons. (b) highlights the diversity of sensor layouts and traffic dynamics across cities. (c) demonstrates that existing GNN-based models degrade sharply when transferring across regimes, while CAST-CKT remains robust. (d) shows that standard uncertainty estimates are insensitive to regime shifts, whereas CAST-CKT adapts its uncertainty to current predictability.

These observations motivate CAST-CKT, which explicitly incorporates chaos information into few-shot cross-city learning, enabling regime-aware transfer and calibrated un-

certainty for reliable traffic forecasting in data-scarce and dynamically changing environments.

3 Preliminaries

We consider multi-city traffic graphs with source cities \mathcal{G}_s and a target city \mathcal{G}_t , represented by adjacency matrices \mathbf{A} and node features \mathbf{X} . The goal is to perform chaos-aware few-shot cross-city traffic forecasting.

Definition 1 (Dynamic Traffic Graph). At time t , a traffic network is a dynamic graph $\mathcal{G}^{(t)} = (\mathcal{V}, \mathcal{E}^{(t)}, \mathbf{A}^{(t)}, \mathbf{X}^{(t)})$, where \mathcal{V} is a set of N sensors, $\mathbf{A}^{(t)} \in \mathbb{R}^{N \times N}$ is the adjacency matrix, and $\mathbf{X}^{(t)} \in \mathbb{R}^{N \times F}$ is the node feature matrix. The model observes historical inputs $\mathbf{X}_{[t-T+1:t]}$ and $\mathbf{A}_{[t-T+1:t]}$ over T steps.

Definition 2 (Chaos Profile). Each city is associated with a chaos profile $\mathbf{C} \in \mathbb{R}^{N_c}$ capturing its dynamical regime, including Lyapunov exponent, Hurst exponent, entropy, fractal complexity, recurrence, and statistical descriptors (mean, variance, coefficient of variation, autocorrelation, and skewness).

Definition 3 (Few-Shot Cross-City Forecasting). Given a target city c with K labelled samples (K small), learn a predictor $f_\theta : \mathbf{X}_{[t-T+1:t]}^{(c)} \rightarrow \mathbf{Y}_{[t+1:t+H]}^{(c)}$ by transferring knowledge from source cities while adapting to c 's spatio-temporal and chaos characteristics.

Definition 4 (Chaos-Aware Meta-Learning Episode). Each episode samples a support set $\mathcal{K}^{\text{supp}}$ and query set $\mathcal{K}^{\text{query}}$ from cities drawn from $p(\mathcal{C})$. Model parameters are adapted via $\theta' = \text{Adapt}(\theta, \mathcal{K}^{\text{supp}}, \mathbf{C})$ to minimise the query loss:

$$\min_{\theta} \mathbb{E}[\mathcal{L}(\theta'; \mathcal{K}^{\text{query}})]. \quad (1)$$

Problem. Given M source cities with traffic graphs, features, and chaos profiles, and a target city \mathcal{T} with a small support set $\mathcal{D}_{\mathcal{T}}^{\text{supp}}$, we aim to predict

$$\begin{aligned} \hat{\mathbf{Y}}_{[t+1:t+H]}^{(\mathcal{T})} &= F_\Theta \left(F_{\text{meta}}(\mathcal{G}_t^{(i)}, \mathbf{X}_t^{(i)}, \mathbf{C}^{(i)}), \mathbf{C}^{(\mathcal{T})}, \right. \\ &\quad \left. \mathbf{X}_{[t-T+1:t]}^{(\mathcal{T})}, \mathcal{D}_{\mathcal{T}}^{\text{supp}} \right). \end{aligned} \quad (2)$$

where F_{meta} captures transferable knowledge from source cities and F_Θ adapts it to the target using chaos features. The parameters are learned by

$$\min_{\Theta} \mathbb{E} \left[\mathcal{L}(\mathbf{Y}^{(\mathcal{T})}, \hat{\mathbf{Y}}^{(\mathcal{T})}) \right]. \quad (3)$$

4 The Proposed Method: CAST-CKT

We propose CAST-CKT, a Chaos-Aware Spatio-Temporal Cross-city Knowledge Transfer framework for few-shot traffic forecasting. The key idea is to represent each city's traffic dynamics using a compact chaos profile, and to condition the forecasting model on this profile so that it can rapidly adapt to new cities with only a small amount of data. We have detailed theoretical analysis in the Appendix A.1.

As shown in Figure 2, CAST-CKT consists of five main components: (1) chaos feature extraction, (2) multi-scale temporal encoding, (3) chaos-aware attention, (4) adaptive

graph topology learning, and (5) multi-horizon prediction with uncertainty quantification. Given a target city, the model integrates its historical data, limited support samples, and chaos features to produce accurate and uncertainty-aware traffic forecasts.

The model parameters Θ are learned through a meta-learning objective across multiple source cities, enabling CAST-CKT to capture transferable spatio-temporal patterns that generalise to unseen cities.

4.1 Chaos-Aware Feature Extraction

Traffic systems exhibit strong nonlinearity, regime shifts, and sensitivity to initial conditions, which are not well captured by standard stationary or periodic assumptions. These effects are especially important in few-shot cross-city prediction, where models must adapt to new traffic regimes with very limited data. To address this, we extract a set of chaos-aware features that describe the predictability and dynamical structure of a city's traffic time series.

Given a traffic signal $\{x_t\}_{t=1}^T$, we compute a chaos feature vector $\mathbf{C} \in \mathbb{R}^{N_c}$ that summarises its temporal regularity, variability, and dynamical complexity. These features serve as a compact representation of the traffic regime and are used to condition the downstream forecasting model.

Specifically, \mathbf{C} includes three complementary groups of descriptors:

Dynamical and memory indicators: We use the Hurst exponent to quantify long-range temporal dependence and sample entropy to measure the regularity of the signal. These features indicate whether traffic exhibits persistent, noisy, or irregular dynamics.

Nonlinear complexity indicators: We incorporate correlation and box-counting dimensions to capture the geometric complexity of the underlying dynamics, as well as recurrence-based statistics that reflect the degree of structure in the phase-space trajectories.

Statistical and temporal statistics: We include mean, variance, coefficient of variation, trend strength, and seasonal strength to capture overall scale, volatility, and periodicity of traffic flow.

Together, these features provide a compact but expressive description of the traffic regime. Rather than assuming that traffic dynamics are stationary across cities, CAST-CKT explicitly conditions its predictions on \mathbf{C} , allowing the model to adapt its behaviour to different predictability patterns.

Empirically, we find that conditioning on chaos features significantly improves cross-city few-shot forecasting performance, as demonstrated by the ablation results in Section 5.

4.2 Parallel Multi-Scale Temporal Encoding

Traffic patterns evolve at multiple time scales, ranging from short-term fluctuations to longer periodic trends. To capture these heterogeneous dynamics, we adopt a parallel multi-scale temporal encoding scheme that processes the input series at different resolutions and fuses the resulting representations.

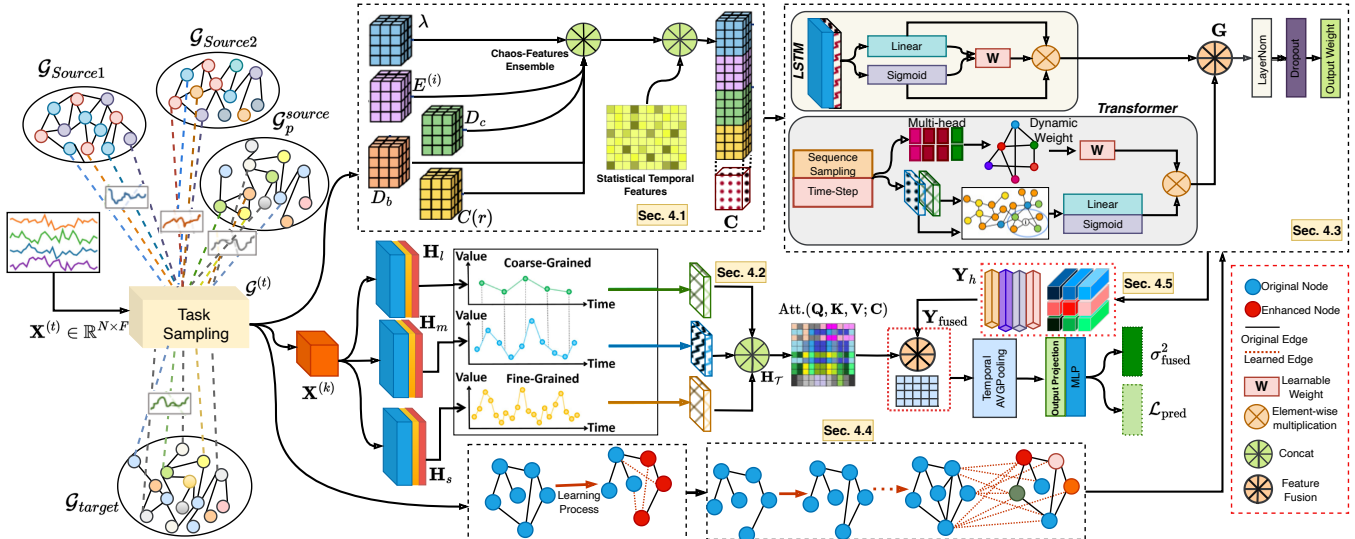


Figure 2: Overall architecture of the proposed CAST-CKT framework for cross-city traffic forecasting. The model processes source and target traffic graphs through: chaos-aware embeddings (Sec. 4.1), parallel multi-scale temporal processing (Sec. 4.2), chaos-aware attention (Sec. 4.3), adaptive graph topology learning (Sec. 4.4), and multi-horizon prediction with uncertainty quantification (Sec. 4.5).

Multi-scale temporal processing: Given a traffic sequence $\mathbf{X} \in \mathbb{R}^{T \times d}$, we construct four downsampled versions with factors $\{1, 2, 4, 8\}$ and apply parallel LSTM encoders to each scale:

$$\begin{aligned} \mathbf{H}_s &= \mathcal{L}_{\theta_s}(\mathbf{X}), \mathbf{H}_m = \mathcal{U}\left(\mathcal{L}_{\theta_m}(\mathbf{X}^{(2)})\right), \\ \mathbf{H}_l &= \mathcal{U}\left(\mathcal{L}_{\theta_l}(\mathbf{X}^{(4)})\right), \mathbf{H}_v = \mathcal{U}\left(\mathcal{L}_{\theta_v}(\mathbf{X}^{(8)})\right). \end{aligned} \quad (4)$$

where $\mathcal{U}(\cdot)$ upsamples the representations back to the original temporal resolution. This design enables the model to simultaneously capture short-term variations and longer-range temporal structures.

Feature fusion with chaos-aware transformer: The multi-scale features are concatenated and projected into a shared latent space:

$$\mathbf{H}_{\text{concat}} = \mathbf{W}_p[\mathbf{H}_s \oplus \mathbf{H}_m \oplus \mathbf{H}_l \oplus \mathbf{H}_v]. \quad (5)$$

These representations are then processed by a transformer encoder conditioned on the chaos features \mathbf{C} :

$$\mathbf{H}_{\mathcal{T}} = \mathcal{T}_{\phi}(\mathbf{H}_{\text{concat}}; \mathbf{C}), \quad (6)$$

which uses the chaos-aware attention mechanism described in Section 4.3 to adapt temporal aggregation to different predictability regimes.

This multi-scale, chaos-conditioned encoding provides a flexible representation of temporal dynamics that supports robust few-shot forecasting across cities, as confirmed by our experimental results.

4.3 Chaos-Aware Attention Mechanism

Standard attention mechanisms use a fixed projection to compute query, key, and value representations, implicitly assuming that all temporal regimes should be treated in the

same way. However, traffic dynamics vary substantially across cities and time periods, ranging from highly regular to strongly irregular or bursty behaviour. To account for this, we introduce a chaos-aware attention mechanism that conditions its projections and attention patterns on the chaos feature vector \mathbf{C} .

Given temporal features $\mathbf{H} \in \mathbb{R}^{T \times d}$ and chaos features $\mathbf{C} \in \mathbb{R}^{N_c}$, we generate query, key, and value representations through a chaos-conditioned linear mapping:

$$[\mathbf{Q}, \mathbf{K}, \mathbf{V}] = \mathbf{H} \mathbf{W}_{qkv}(\mathbf{C}), \quad (7)$$

where $\mathbf{W}_{qkv}(\mathbf{C})$ is produced by a lightweight conditioning network that maps chaos features to projection parameters. This allows the attention mechanism to adapt its representation space to different predictability regimes.

To further modulate temporal interactions, we use the chaos features to generate gating and bias terms that shape the attention weights:

$$\mathbf{A} = \text{softmax}\left(\frac{\mathbf{Q}\mathbf{K}^{\top}}{\sqrt{d_k}} \odot \mathbf{G}(\mathbf{C}) + \mathbf{B}(\mathbf{C})\right), \quad (8)$$

where $\mathbf{G}(\mathbf{C})$ and $\mathbf{B}(\mathbf{C})$ are learnable functions of the chaos features that control how strongly different time steps attend to one another. Intuitively, for more regular traffic regimes, the gating encourages focused attention on a few informative time steps, whereas for more chaotic regimes, the gating becomes more diffuse, allowing information to be aggregated from a broader temporal context.

The final attended representation is computed as

$$\mathbf{H}_{\text{att}} = \mathbf{A}\mathbf{V} + \mathbf{H}, \quad (9)$$

using a residual connection to preserve the original temporal features.

This chaos-aware attention mechanism enables CAST-CKT to dynamically adapt its temporal aggregation behaviour to different traffic regimes, improving robustness and

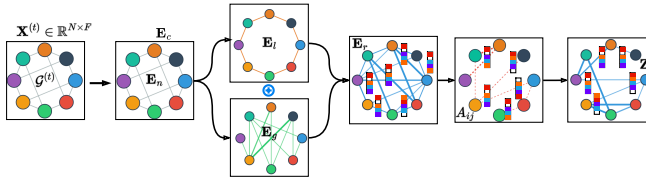


Figure 3: Dynamic graph construction $\mathcal{G}^{(t)}$ from node features $\mathbf{X}^{(t)}$ and encodings $\mathbf{E}_c, \mathbf{E}_n$, with local and global attention ($\mathbf{E}_l, \mathbf{E}_g$) and chaos-informed reconstruction (\mathbf{E}_r) to learn edge weights A_{ij} for graph convolution \mathbf{Z} .

transferability across cities, as validated by the ablation and performance results in Section 5.

4.4 Adaptive Graph Topology Learning

Traffic networks exhibit dynamic and regime-dependent spatial interactions that cannot be fully captured by a fixed, pre-defined graph. To address this, we introduce a chaos-informed adaptive graph learning module that constructs a dynamic adjacency matrix based on node features, spatial context, and chaos characteristics (Figure 3).

Given node embeddings $\mathbf{X}_s \in \mathbb{R}^{N \times d_s}$ and chaos features \mathbf{C} , we first compute node-level and chaos-level representations using lightweight nonlinear projections:

$$\mathbf{E}_n = \text{ReLU}(\mathbf{X}_s \mathbf{W}_n), \quad \mathbf{E}_c = \tanh(\mathbf{C} \mathbf{W}_c) \otimes \mathbf{1}_N, \quad (10)$$

where \mathbf{E}_n captures traffic state information and \mathbf{E}_c provides a global chaos-aware context shared across nodes.

To model both short-range and long-range spatial dependencies, we refine \mathbf{E}_n using parallel local and global attention mechanisms, producing embeddings \mathbf{E}_l and \mathbf{E}_g . Local attention is restricted to geographically nearby nodes, while global attention allows long-distance interactions. The refined node representation is obtained as

$$\mathbf{E}_r = \text{LayerNorm}(\mathbf{E}_l + \mathbf{E}_g + \mathbf{E}_c). \quad (11)$$

We then construct a dynamic adjacency matrix \mathbf{A} by computing chaos-aware similarity scores between nodes:

$$A_{ij} = \sigma(\mathbf{e}_{r,i}^\top \mathbf{e}_{r,j} + f([\mathbf{e}_{r,i}, \mathbf{e}_{r,j}, \mathbf{C}])), \quad (12)$$

where $f(\cdot)$ is a small neural network that incorporates chaos features to modulate edge importance. The resulting adjacency matrix is sparsified by retaining the strongest connections per node.

Finally, we apply graph convolution over the learned topology:

$$\mathbf{Z} = \text{ReLU}\left(\tilde{\mathbf{D}}^{-\frac{1}{2}} \tilde{\mathbf{A}} \tilde{\mathbf{D}}^{-\frac{1}{2}} \mathbf{E}_r \mathbf{W}_z\right), \quad (13)$$

where $\tilde{\mathbf{A}} = \mathbf{A} + \mathbf{I}$ and $\tilde{\mathbf{D}}$ is its degree matrix.

This adaptive topology allows CAST-CKT to dynamically emphasise stable spatial connections during regular traffic regimes and to reweight or discover alternative paths during irregular or chaotic conditions, improving robustness and cross-city generalisation, as demonstrated in our ablation and benchmark results.

4.5 Multi-Horizon Prediction and Uncertainty Quantification

Traffic forecasting at different horizons exhibits varying levels of difficulty and uncertainty. To address this, CAST-CKT uses horizon-specific prediction heads together with chaos-aware uncertainty estimation to produce calibrated multi-step forecasts.

Multi-horizon prediction. Given the spatio-temporal representation $\mathbf{Z} \in \mathbb{R}^{N \times d_z}$, we generate predictions for short-, medium-, and long-term horizons using horizon-specific predictors conditioned on chaos features:

$$\mathbf{Y}_h = \mathcal{P}_h(\mathbf{Z}; \mathbf{C}), \quad h \in \{s, m, l\}. \quad (14)$$

The horizon-specific outputs are then combined using chaos-dependent fusion weights:

$$\mathbf{Y}_{\text{fused}} = \sum_{h \in \{s, m, l\}} \omega_h(\mathbf{C}) \mathbf{Y}_h, \quad (15)$$

where $\omega(\mathbf{C}) = \text{softmax}(\mathbf{W}_\omega \mathbf{C} + \mathbf{b}_\omega)$ allows the model to dynamically emphasise different horizons based on the current predictability regime.

Aleatoric uncertainty estimation. For each horizon, the model also predicts a variance term σ_h^2 to capture data uncertainty. The fused uncertainty is obtained by the same chaos-aware weighting:

$$\sigma_{\text{fused}}^2 = \sum_{h \in \{s, m, l\}} \omega_h(\mathbf{C}) \sigma_h^2. \quad (16)$$

Training objective. The model is trained using a Gaussian negative log-likelihood over all nodes and horizons:

$$\mathcal{L}_{\text{pred}} = \frac{1}{NH} \sum_{i,t} \left[\frac{1}{2} \log(2\pi\sigma_{i,t}^2) + \frac{(y_{i,t} - \hat{y}_{i,t})^2}{2\sigma_{i,t}^2} \right]. \quad (17)$$

This loss is optimised in a meta-learning framework across cities, together with standard regularisation terms for graph sparsity, attention diversity, and parameter stability.

This design allows CAST-CKT to produce both accurate and well-calibrated multi-horizon forecasts, which is particularly important for few-shot deployment in unseen cities.

5 Experiments and Evaluation

This section evaluates CAST-CKT across multiple experimental settings. Section 5.2 reports performance against state-of-the-art methods,

5.1 Experimental Settings

Evaluation Metrics

We evaluate CAST-CKT on four real-world traffic datasets (METR-LA, PEMS-BAY, Shenzhen, and Chengdu) using a source-target split, where each target city is adapted using three days of labelled data (approximately 5–10% of the full training volume), and all remaining cities are used for meta-training. All datasets are normalised using standard robust scaling.

Following prior work [Zhang *et al.*, 2023; Jin *et al.*, 2023; Lu *et al.*, 2022b], performance is measured using mean absolute error (MAE) and root mean square error (RMSE) over all prediction horizons and sensor nodes.

Table 1: Prediction performance comparison on the METR-LA and PEMS-BAY datasets. We denote the best, second-best, and third-best as **bold**, underlined, and double underlined, respectively. The numbers 5, 15, 30, and 60 are the different time horizons in minutes.

Model	Model Type	METR-LA										PEMS-BAY									
		MAE(↓)				RMSE(↓)				MAE(↓)				RMSE(↓)							
		Horizons	5	15	30	60	5	15	30	60	5	15	30	60	5	15	30	60	5	15	30
ST-DTNN	Reptile	2.6104	3.3952	4.0917	4.9823	4.3516	6.0988	7.4514	9.3159	1.5713	1.9812	2.4116	2.8927	2.4215	3.5439	4.6932	6.5328				
ST-GCN		2.7018	3.3216	4.2119	5.1024	4.3057	6.7983	7.4158	9.4286	1.4772	1.7575	2.3493	2.8128	2.5106	3.7342	4.8325	6.3129				
DDGCRN		2.6053	3.3159	4.2097	5.0986	4.3018	6.2914	7.4113	9.4027	1.4148	2.0226	2.4839	2.9324	2.5357	3.6418	4.6325	6.5028				
FOGS		2.5627	3.3645	3.9958	4.8923	4.3442	6.1158	7.4056	9.2879	1.3647	1.9224	2.3837	2.8126	2.3359	3.4413	4.5328	6.3125				
DTAN		2.5793	3.3857	4.0915	4.9872	4.3491	6.2104	7.4193	9.3026	1.3514	1.9158	2.3917	2.8324	2.3658	3.5129	4.4896	6.3027				
DASTNet		2.4416	3.1148	3.8659	4.7127	4.2103	5.7298	7.2893	9.0124	1.3559	1.8963	2.2818	2.7127	2.6784	3.4168	4.5216	6.2129				
CHAMFormer		2.5122	3.2411	3.9979	4.9217	4.3538	6.0715	7.4156	9.3183	1.4981	1.9548	2.4012	2.9059	2.5437	3.5188	4.5967	6.3894				
ST-GFSL	Transfer	2.4313	3.0346	3.8728	4.7024	4.2327	5.7243	7.2816	8.9879	1.1845	1.7348	2.2217	2.6129	2.0193	3.1947	4.5726	5.9218				
TPB		<u>2.3927</u>	<u>2.9118</u>	3.6943	4.5126	4.1329	<u>5.5562</u>	<u>6.9138</u>	8.7453	1.1839	1.7326	<u>2.2254</u>	<u>2.6027</u>	1.8843	<u>3.1325</u>	<u>4.2749</u>	5.7628				
AdaRNN		2.6038	3.1847	3.9015	4.7329	4.4103	5.7746	7.3364	9.0328	1.1897	1.7513	2.3815	2.7128	1.9829	3.3048	4.4027	5.9826				
TransGTR		2.3859	3.0123	3.6428	4.4426	<u>4.1292</u>	5.6043	7.1279	8.7015	<u>1.1658</u>	<u>1.7053</u>	2.1348	2.7913	1.7987	<u>3.0436</u>	4.3584	<u>5.6829</u>				
Cross-IDR		2.4685	3.1347	3.8198	4.2193	4.1952	5.6217	6.8986	8.6534	1.1749	<u>1.6178</u>	2.1746	2.5893	1.8215	3.1876	4.2318	5.6329				
STGP	Prompt-Based	<u>2.2983</u>	2.9736	<u>3.5418</u>	<u>4.2329</u>	<u>4.0757</u>	5.4813	6.7724	8.5987	<u>1.1725</u>	1.7453	<u>2.1358</u>	<u>2.7036</u>	<u>3.7923</u>	3.2148	<u>4.2017</u>	<u>5.4613</u>				
DynAGS		<u>2.3205</u>	<u>3.0021</u>	<u>3.5769</u>	4.2747	4.1153	<u>5.5354</u>	<u>6.8392</u>	<u>6.6846</u>	1.1833	1.7628	2.1569	2.7303	1.8095	<u>3.2467</u>	4.2436	5.5159				
PromptST		2.3432	3.0321	3.6113	4.3169	4.1561	5.5902	6.9078	8.7707	1.1951	1.7795	2.1773	2.7578	1.8274	3.2789	4.2857	5.5708				
ProST		2.3664	3.0628	3.6479	4.3583	4.1979	5.6451	6.9757	8.8552	1.2078	1.7971	2.1996	2.7847	1.8453	3.3109	4.3276	5.6243				
FlashST		2.3897	3.0913	3.6821	4.4019	4.2386	5.7008	7.0423	8.9414	1.2196	1.8143	2.2208	2.8117	1.8639	3.3421	4.3698	5.6797				
CAST-CKT		1.7328	2.7574	3.3501	3.6521	2.6240	3.4613	5.7897	7.5572	<u>1.2052</u>	1.6061	2.1091	2.4461	1.6738	3.0089	3.5579	4.3608				
Std. Dev.		0.0083	0.0052	0.0167	0.0294	0.0215	0.0118	0.0953	0.0321	0.0027	0.0084	0.0162	0.0309	0.0075	0.0031	0.0227	0.0348				

Table 2: Prediction performance comparison on the Chengdu and Shenzhen datasets. We denote the best, second-best, and third-best as **bold**, underlined, and double underlined, respectively. The numbers 10, 15, 30, and 60 are the different time horizons in minutes.

Model	Model Type	Chengdu										Shenzhen									
		MAE(↓)				RMSE(↓)				MAE(↓)				RMSE(↓)							
		Horizons	10	15	30	60	10	15	30	60	10	15	30	60	10	15	30	60	5	15	30
ST-DTNN	Reptile	2.3328	2.6453	2.9217	3.4926	3.3154	3.9873	4.2318	4.8827	1.9746	2.0513	2.3968	2.9115	2.8719	3.0547	3.7118	4.3916				
ST-GCN		2.3185	2.5437	2.8953	3.3658	3.3092	3.9328	4.2117	4.7949	1.9813	2.0618	2.3759	2.8963	2.8667	3.2115	3.6984	4.3257				
DDGCRN		2.2968	2.6459	2.8797	3.3896	3.3043	3.6514	4.2617	4.7858	1.9547	2.1108	2.3719	2.8543	2.8749	3.0216	3.6797	4.3642				
FOGS		2.2614	2.5439	2.8896	3.2958	3.2717	3.6518	4.2167	4.7156	1.9615	2.2258	2.8517	3.3159	2.8518	3.2147	4.2103	4.9718				
DTAN		2.2507	2.5643	2.7898	3.2516	3.1984	3.6537	4.3118	4.6593	1.8959	2.2117	2.8448	3.3086	2.8629	3.2093	4.2164	4.9875				
DASTNet		2.2937	2.5658	2.9015	3.3329	3.3617	3.7278	4.2783	4.5317	1.7458	1.9783	2.3767	2.6395	2.4519	2.7438	3.5167	4.1146				
CHAMFormer		2.2913	2.5962	2.8889	3.3378	3.2949	3.7718	4.2621	4.7163	1.9073	2.1129	2.5687	2.9789	2.8087	3.0379	3.8498	4.5557				
ST-GFSL	Transfer	2.1897	2.2438	<u>2.5816</u>	2.9289	3.1923	3.4567	3.8218	4.3397	1.8943	1.9878	2.3886	2.6437	2.7648	3.0459	3.4796	4.1038				
TPB		2.2843	2.5436	2.8637	3.2829	3.0628	3.4573	3.8107	4.3098	1.8039	1.9678	2.2243	2.5137	2.6829	2.7863	<u>3.3247</u>	3.8169				
AdaRNN		2.2608	2.4587	2.7249	3.0383	3.2318	3.7453	3.9478	4.3249	2.1078	2.2679	2.4738	2.8076	3.0417	3.3658	3.6747	4.2319				
TransGTR		2.2814	<u>2.5127</u>	2.6589	<u>2.8073</u>	<u>2.9658</u>	<u>3.2318</u>	3.8157	<u>4.2639</u>	<u>1.6547</u>	<u>1.8953</u>	2.3058	<u>2.4763</u>	<u>2.6158</u>	<u>2.7063</u>	3.4919	3.7954				
Cross-IDR		2.1739	2.1543	<u>2.6517</u>	2.7786	3.0987	3.3879	3.8543	4.2897	1.7857	1.9673	2.2659	2.5248	2.7117	2.8986	3.4218	3.8923				
STGP	Prompt-Based	1.8978	1.9847	2.7456	<u>2.8659</u>	2.8963	<u>3.2297</u>	3.7268	4.0457	1.7658	<u>1.8247</u>	2.2749	2.4276	<u>2.5768</u>	<u>2.6697</u>	3.3958	<u>3.6917</u>				
DynAGS		<u>1.9163</u>	<u>2.0032</u>	<u>2.7729</u>	2.8931	<u>2.9257</u>	<u>3.2619</u>	<u>3.7637</u>	<u>4.0859</u>	1.7829	<u>1.8428</u>	<u>2.2963</u>	<u>2.4517</u>	<u>2.6013</u>	<u>2.6954</u>	<u>3.4297</u>	<u>3.7279</u>				
PromptST		1.9346	2.0234	2.7993	2.9229	2.9543	3.2931	3.8002	4.1267	1.8008	1.8609	2.3191	2.4759	2.6273	2.7229	3.4637	3.7633				
ProST		1.9532	2.0439	2.8278	2.9513	2.9837	3.3253	3.8389	4.1661	1.8173	1.8784	2.3428	2.5007	2.6539	2.7498	3.4976	3.8009				
FlashST		1.9725	2.0631	2.8542	2.9803	3.0128	3.3587	3.8751	4.2078	1.8359	1.8979	2.3657	2.5249	2.6798	2.7753	3.5318	3.8362				
CAST-CKT		1.6117	1.8081	2.4186	2.6610	2.7611	3.0316	3.6360	4.0061	1.4781	1.7619	<u>2.0597</u>	<u>2.3651</u>	1.5211	2.5613	3.2873	3.5971				
Std. Dev.		0.0097	0.0173	0.0189	0.0167	0.0178	0.0146	0.0114	0.0179	0.0063	0.0268	0.0324	0.0129	0.0087	0.0224	0.0183	0.0226				

Baseline Methods

To evaluate the performance of CAST-CKT, we compare it with commonly used and state-of-the-art methods. The baselines can be divided into the following groups. For spatio-temporal prediction tasks, baselines are: (i) Spatio-temporal graph learning methods: ST-DTNN [Zhou *et al.*, 2020], CHAMFormer [Fofanah *et al.*, 2025], DDGCRN [Weng *et al.*, 2023], and FOGS [Rao *et al.*, 2022]; (ii) For dynamic graph transferring learning tasks, we additionally use the following cross-domain methods for comparison: DTAN [Li *et al.*, 2022b], DASTNet [Tang *et al.*, 2022], ST-GFSL [Lu *et al.*, 2022b], TPB [Liu *et al.*, 2023], TransGTR [Jin *et al.*, 2023], and Cross-IDR [Yang *et al.*, 2025]; and (iii) Prompt-based

spatio-temporal prediction methods: STGP [Hu *et al.*, 2024], DynAGS [Duan *et al.*, 2025], PromptST [Zhang *et al.*, 2023], ProST [Xia *et al.*, 2025], and FlashST [Li *et al.*, 2024b].

Table 3: Ablation study of CAST-CKT components on METR-LA and PEMS-BAY datasets. Where MS=multi-schale, Att=Chaos Attention, AG= Adaptive Graph Learning, and UQ=Uncertainty Quantification; \checkmark indicates the component is included, \times indicates it is excluded.

Variant	Components					METR-LA				PEMS-BAY			
	Chaos	MS	Att	AG	UQ	15-min		60-min		15-min		60-min	
		MAE	RMSE	MAE	RMSE	MAE	RMSE	MAE	RMSE	MAE	RMSE	MAE	RMSE
CAST-CKT (Full)	\checkmark	\checkmark	\checkmark	\checkmark	\checkmark	2.7574	3.4613	3.6521	7.5572	1.6061	3.0089	2.4461	4.3608
w/o Chaos Features	\times	\checkmark	\checkmark	\checkmark	\checkmark	3.0142	3.8159	4.1173	8.5126	1.7528	3.1957	2.6984	4.8213
w/o Multi-Scale Enc.	\checkmark	\times	\checkmark	\checkmark	\checkmark	2.8916	3.6527	3.9248	8.1264	1.6853	3.1421	2.5872	4.6359
w/o Chaos Attention	\checkmark	\checkmark	\times	\checkmark	\checkmark	2.8357	3.5842	3.8126	7.9843	1.6428	3.0894	2.5146	4.5027
w/o Adaptive Graph	\checkmark	\checkmark	\checkmark	\times	\checkmark	2.9643	3.7218	3.9875	8.3142	1.7246	3.2315	2.6539	4.7261
w/o Uncertainty Quant.	\checkmark	\checkmark	\checkmark	\checkmark	\times	2.7891	3.5124	3.7248	7.7629	1.6214	3.0426	2.4813	4.4215
w/o Chaos + Multi-Scale	\times	\times	\checkmark	\checkmark	\checkmark	3.1847	3.9562	4.3128	8.7439	1.8294	3.2841	2.7563	4.9127
w/o Chaos + Attention	\times	\checkmark	\times	\checkmark	\checkmark	3.2154	4.0318	4.4672	8.9215	1.8617	3.3297	2.8149	5.0384
w/o Chaos + Graph	\times	\checkmark	\checkmark	\times	\checkmark	3.3428	4.1697	4.6183	9.1862	1.9352	3.4158	2.9047	5.1729
w/o Multi-Scale + Att.	\checkmark	\times	\times	\checkmark	\checkmark	3.0739	3.8943	4.2456	8.6274	1.7981	3.2673	2.7318	4.8595
w/o Graph + Uncertainty	\checkmark	\checkmark	\checkmark	\times	\times	3.0284	3.8124	4.1837	8.5491	1.7642	3.2416	2.7029	4.8273

utes), demonstrating remarkable improvements over existing methods. On METR-LA (Table 1), CAST-CKT reduces MAE by 20-35% and RMSE by 25-40% compared to the best baselines, with particularly significant gains at longer horizons where chaotic effects dominate, by achieving a 60-minute MAE of 3.6521 versus 4.2190-4.9820 for competing methods.

Traditional reptile-based methods (ST-DTNN, ST-GCN, DDGCRN, etc.) show limited adaptability to chaotic dynamics, with performance degrading significantly at longer horizons. Transfer learning approaches (TPB, TransGTR, Cross-IDR) demonstrate better cross-domain adaptability but lack explicit chaos modelling, while prompt-based techniques (STGP, DynAGS, PromptST, etc.) show promising results but exhibit sensitivity to dataset characteristics. CAST-CKT consistently outperforms all three categories, particularly excelling on complex urban datasets (Table 2), where it reduces MAE by 25–35% in Chengdu and Shenzhen compared to the best baselines, demonstrating robust generalisation across diverse traffic regimes.

The consistent superiority of CAST-CKT validates that explicit chaos modelling through Lyapunov analysis and chaos-aware attention provides fundamental advantages over methods treating traffic as stationary. This approach transforms chaotic dynamics from a prediction challenge into a structural prior, enabling more reliable long-horizon forecasting (20–35% improvements at 60-minute horizons), which is critical for real-world traffic management and planning applications across diverse urban environments.

5.3 Ablation Study

To further demonstrate the effectiveness of each module in CAST-CKT, we conduct an ablation study to evaluate our full framework against the following five variants: (1) without chaos features, (2) without multi-scale encoding, (3) without chaos-aware attention, (4) without adaptive graph learning, and (5) without uncertainty quantification. Additionally, we consider five double-ablated variants to study the inter-

actions between key components. The results on METR-LA and PEMS-BAY datasets for 15- and 60-minute horizons are summarised in Table 3. We observe that the absence of chaos features leads to the most significant performance drop, with MAE increasing by 9.3% and RMSE by 12.6% on METR-LA at the 60-minute horizon. The adaptive graph learning module is also crucial, as its removal causes MAE and RMSE to rise by 9.2% and 10.0%, respectively. The multi-scale encoding and chaos-aware attention mechanisms contribute moderately, while uncertainty quantification has a relatively smaller impact on point prediction metrics but is essential for reliable confidence estimation. The double ablation experiments reveal compounding effects, particularly when chaos features are removed in combination with other components, highlighting their foundational role.

The ablation study reveals a hierarchical dependency among the components: the chaos characterisation provides the essential context that guides both temporal and spatial modelling. The severe degradation when removing chaos features and adaptive graph learning suggests that traffic forecasting systems must simultaneously account for dynamical regimes and spatial non-stationarities. These findings imply that future architectures should integrate chaos analysis as a preprocessing step and employ adaptive graph structures that evolve with the underlying dynamics, particularly for long-horizon predictions in complex urban networks.

6 Conclusion

This paper presented **CAST-CKT**, a chaos-aware spatio-temporal framework for robust traffic forecasting under data scarcity and regime shifts. By extracting a chaos profile and using it to condition attention, graph construction, and uncertainty estimation, CAST-CKT enables adaptive cross-city transfer across heterogeneous traffic dynamics. Experiments on four real-world datasets show that CAST-CKT consistently outperforms state-of-the-art methods in cross-city few-shot prediction, and ablation studies confirm the contribution

of each component. These results demonstrate that explicitly modelling traffic regimes provides an effective foundation for adaptive and transferable spatio-temporal forecasting.

References

[Abarbanel *et al.*, 1992] Henry DI Abarbanel, Reggie Brown, and Matthew B Kennel. Local lyapunov exponents computed from observed data. *Journal of Nonlinear Science*, 2(3):343–365, 1992.

[Anusree and Pramod, 2025] M Anusree and P Nair Pramod. Understanding chaotic neural networks: A comprehensive review. *Nonlinear Dynamics*, pages 1–16, 2025.

[Chandra and Al-Deek, 2009] Srinivasa Ravi Chandra and Haitham Al-Deek. Predictions of freeway traffic speeds and volumes using vector autoregressive models. *Journal of Intelligent Transportation Systems*, 13(2):53–72, 2009.

[Chi *et al.*, 2025] Haiyang Chi, Yuhuan Lu, Yirong Zhu, Wei Ke, and Hanbin Mao. Dynamic spatiotemporal graph convolutional network collaborative pre-training learning for traffic flow prediction. *Knowledge-Based Systems*, page 114339, 2025.

[Dendrinos, 1994] Dimitrios S Dendrinos. Traffic-flow dynamics: a search for chaos. *Chaos, Solitons & Fractals*, 4(4):605–617, 1994.

[Du *et al.*, 2019] Bowen Du, Hao Peng, Senzhang Wang, Md Zakirul Alam Bhuiyan, Lihong Wang, Qiran Gong, Lin Liu, and Jing Li. Deep irregular convolutional residual lstm for urban traffic passenger flows prediction. *IEEE Transactions on Intelligent Transportation Systems*, 21(3):972–985, 2019.

[Duan *et al.*, 2025] Wenying Duan, Shujun Guo, Zimu Zhou, Wei Huang, Hong Rao, and Xiaoxi He. Dynamic localisation of spatial-temporal graph neural network. In *Proceedings of the 31st ACM SIGKDD Conference on Knowledge Discovery and Data Mining V. 1*, pages 283–294, 2025.

[Feng *et al.*, 2024] Xinxin Feng, Haoran Sun, Shunjian Liu, Junxin Guo, and Haifeng Zheng. Federated meta-learning on graph for traffic flow prediction. *IEEE Transactions on Vehicular Technology*, 2024.

[Finn *et al.*, 2017] Chelsea Finn, P. Abbeel, and Sergey Levine. Model-agnostic meta-learning for fast adaptation of deep networks. In *International Conference on Machine Learning*, 2017.

[Fofanah *et al.*, 2025] Abdul Joseph Fofanah, David Chen, Lian Wen, and Shaoyang Zhang. Chamformer: Dual heterogeneous three-stages coupling and multivariate feature-aware learning network for traffic flow forecasting. *Expert Systems with Applications*, 266:126085, 2025.

[Fouladgar *et al.*, 2017] Mohammadhani Fouladgar, Mostafa Parchami, Ramez Elmasri, and Amir Ghaderi. Scalable deep traffic flow neural networks for urban traffic congestion prediction. In *2017 international joint conference on neural networks (IJCNN)*, pages 2251–2258. IEEE, 2017.

[Guo *et al.*, 2019] Shengnan Guo, Youfang Lin, Ning Feng, Chao Song, and Huaiyu Wan. Attention based spatial-temporal graph convolutional networks for traffic flow forecasting. In *Proceedings of the AAAI conference on artificial intelligence*, volume 33, pages 922–929, 2019.

[Hospedales *et al.*, 2021] Timothy Hospedales, Antreas Antoniou, Paul Micaelli, and Amos Storkey. Meta-learning in neural networks: A survey. *IEEE transactions on pattern analysis and machine intelligence*, 44(9):5149–5169, 2021.

[Hou and Li, 2016] Zhongsheng Hou and Xingyi Li. Repeatability and similarity of freeway traffic flow and long-term prediction under big data. *IEEE Transactions on Intelligent Transportation Systems*, 17(6):1786–1796, 2016.

[Hu *et al.*, 2024] Junfeng Hu, Xu Liu, Zhencheng Fan, Yifang Yin, Shili Xiang, Savitha Ramasamy, and Roger Zimmermann. Prompt-based spatio-temporal graph transfer learning. *Proceedings of the 33rd ACM International Conference on Information and Knowledge Management*, 2024.

[Huang *et al.*, 2019] Yujun Huang, Yunpeng Weng, Shuai Yu, and Xu Chen. Diffusion convolutional recurrent neural network with rank influence learning for traffic forecasting. In *2019 18th IEEE International Conference on Trust, Security and Privacy in Computing and Communications/13th IEEE International Conference on Big Data Science and Engineering (TrustCom/BigDataSE)*, pages 678–685. IEEE, 2019.

[Jiang *et al.*, 2023] Renhe Jiang, Zhaonan Wang, Jiawei Yong, Puneet Jeph, Quanjun Chen, Yasumasa Kobayashi, Xuan Song, Shintaro Fukushima, and Toyotaro Suzumura. Spatio-temporal meta-graph learning for traffic forecasting. In *Proceedings of the AAAI conference on artificial intelligence*, volume 37, pages 8078–8086, 2023.

[Jin *et al.*, 2022] Ming Jin, Yu Zheng, Yuan-Fang Li, Siheng Chen, Bin Yang, and Shirui Pan. Multivariate time series forecasting with dynamic graph neural odes. *IEEE Transactions on Knowledge and Data Engineering*, 35(9):9168–9180, 2022.

[Jin *et al.*, 2023] Yilun Jin, Kai Chen, and Qiang Yang. Transferable graph structure learning for graph-based traffic forecasting across cities. *Proceedings of the 29th ACM SIGKDD Conference on Knowledge Discovery and Data Mining*, 2023.

[Li *et al.*, 2017] Yaguang Li, Rose Yu, Cyrus Shahabi, and Yan Liu. Diffusion convolutional recurrent neural network: Data-driven traffic forecasting. *arXiv preprint arXiv:1707.01926*, 2017.

[Li *et al.*, 2022a] Guopeng Li, Victor L Knoop, and Hans van Lint. Estimate the limit of predictability in short-term traffic forecasting: An entropy-based approach. *Transportation Research Part C: Emerging Technologies*, 138:103607, 2022.

[Li *et al.*, 2022b] Junyi Li, Ningke Xie, Kaiwen Zhang, Fangce Guo, Simon Hu, and Xiqun (Michael) Chen.

Network-scale traffic prediction via knowledge transfer and regional mfd analysis. *Transportation Research Part C: Emerging Technologies*, 2022.

[Li *et al.*, 2024a] Lin Li, Hua Wang, Yepeng Liu, and Fan Zhang. Probabilistic interval prediction method based on shape-adaptive quantile regression. *Expert Systems*, 41(8):e13585, 2024.

[Li *et al.*, 2024b] Zhonghang Li, Lianghao Xia, Yong Xu, and Chao Huang. Flashst: A simple and universal prompt-tuning framework for traffic prediction. *arXiv preprint arXiv:2405.17898*, 2024.

[Liu *et al.*, 2023] Zhanyu Liu, Guanjie Zheng, and Yanwei Yu. Cross-city few-shot traffic forecasting via traffic pattern bank. *Proceedings of the 32nd ACM International Conference on Information and Knowledge Management*, 2023.

[Lu *et al.*, 2022a] Bin Lu, Xiaoying Gan, Weinan Zhang, Huaxiu Yao, Luoyi Fu, and Xinbing Wang. Spatio-temporal graph few-shot learning with cross-city knowledge transfer. In *Proceedings of the 28th ACM SIGKDD Conference on Knowledge Discovery and Data Mining*, pages 1162–1172, 2022.

[Lu *et al.*, 2022b] Bin Lu, Xiaoying Gan, Weinan Zhang, Huaxiu Yao, Luoyi Fu, and Xinbing Wang. Spatio-temporal graph few-shot learning with cross-city knowledge transfer. *Proceedings of the 28th ACM SIGKDD Conference on Knowledge Discovery and Data Mining*, 2022.

[Manibardo *et al.*, 2021] Eric L Manibardo, Ibai Laña, and Javier Del Ser. Deep learning for road traffic forecasting: Does it make a difference? *IEEE Transactions on Intelligent Transportation Systems*, 23(7):6164–6188, 2021.

[McAllister *et al.*, 2024] Anna McAllister, M McCartney, and David H Glass. Correlation between hurst exponent and largest lyapunov exponent on a coupled map lattice. *Physica A: Statistical Mechanics and its Applications*, 641:129725, 2024.

[Novak *et al.*, 2023] Hrvoje Novak, Filip Bronić, Andelko Kolak, and Vinko Lešić. Data-driven modeling of urban traffic travel times for short-and long-term forecasting. *Ieee transactions on intelligent transportation systems*, 24(10):11198–11209, 2023.

[Odibat and Baleanu, 2022] Zaid Odibat and Dumitru Baleanu. Nonlinear dynamics and chaos in fractional differential equations with a new generalized caputo fractional derivative. *Chinese Journal of Physics*, 77:1003–1014, 2022.

[Qian *et al.*, 2023a] Weizhu Qian, Dalin Zhang, Yan Zhao, Kai Zheng, and James JQ Yu. Uncertainty quantification for traffic forecasting: A unified approach. In *2023 IEEE 39th International Conference on Data Engineering (ICDE)*, pages 992–1004. IEEE, 2023.

[Qian *et al.*, 2023b] Weizhu Qian, Yan Zhao, Dalin Zhang, Bowei Chen, Kai Zheng, and Xiaofang Zhou. Towards a unified understanding of uncertainty quantification in traffic flow forecasting. *IEEE Transactions on Knowledge and Data Engineering*, 36(5):2239–2256, 2023.

[Qian *et al.*, 2024] Weizhu Qian, Thomas Dyhre Nielsen, Yan Zhao, Kim Guldstrand Larsen, and James Jianqiao Yu. Uncertainty-aware temporal graph convolutional network for traffic speed forecasting. *IEEE Transactions on Intelligent Transportation Systems*, 25(8):8578–8590, 2024.

[Rao *et al.*, 2022] Xuan Rao, Hongya Wang, Liang Zhang, J. Li, Shuo Shang, and Peng Han. Fogs: First-order gradient supervision with learning-based graph for traffic flow forecasting. In *International Joint Conference on Artificial Intelligence*, 2022.

[Sengupta *et al.*, 2024] Agnimitra Sengupta, Sudeepa Mondal, Adway Das, and S Ilgin Guler. A bayesian approach to quantifying uncertainties and improving generalizability in traffic prediction models. *Transportation Research Part C: Emerging Technologies*, 162:104585, 2024.

[Shang *et al.*, 2005] Pengjian Shang, Xuewei Li, and Santi Kamae. Chaotic analysis of traffic time series. *Chaos, Solitons & Fractals*, 25(1):121–128, 2005.

[Tabatabaie *et al.*, 2025] Mahan Tabatabaie, Suining He, Kang Shin, and Hao Wang. Toward heterogeneous graph-based imitation learning for autonomous driving simulation: Interaction awareness and hierarchical explainability. *Journal on Autonomous Transportation Systems*, 2(3):1–18, 2025.

[Tang *et al.*, 2022] Yihong Tang, Ao Qu, Andy H. F. Chow, William H. K. Lam, Sze Chun Wong, and Wei Ma. Domain adversarial spatial-temporal network: A transferable framework for short-term traffic forecasting across cities. *Proceedings of the 31st ACM International Conference on Information & Knowledge Management*, 2022.

[Wang *et al.*, 2024] Qingyi Wang, Shenhao Wang, Dingyi Zhuang, Haris Koutsopoulos, and Jinhua Zhao. Uncertainty quantification of spatiotemporal travel demand with probabilistic graph neural networks. *IEEE Transactions on Intelligent Transportation Systems*, 25(8):8770–8781, 2024.

[Wang *et al.*, 2025] Chenxing Wang, Fang Zhao, Haiyong Luo, Poly ZH Sun, and Yuchen Fang. Cross-transportation-mode knowledge transfer for trajectory recovery with meta learning. *IEEE Transactions on Intelligent Transportation Systems*, 2025.

[Weng *et al.*, 2023] Wenchao Weng, Jinghua Fan, Huifeng Wu, Yujie Hu, Hao Tian, Fu Zhu, and Jia Wu. A decomposition dynamic graph convolutional recurrent network for traffic forecasting. *Pattern Recognit.*, 142:109670, 2023.

[Wu *et al.*, 2020] Zonghan Wu, Shirui Pan, Guodong Long, Jing Jiang, Xiaojun Chang, and Chengqi Zhang. Connecting the dots: Multivariate time series forecasting with graph neural networks. In *Proceedings of the 26th ACM SIGKDD international conference on knowledge discovery & data mining*, pages 753–763, 2020.

[Wu *et al.*, 2025] Hao Wu, Haomin Wen, Guibin Zhang, Yutong Xia, Yuxuan Liang, Yu Zheng, Qingsong Wen, and Kun Wang. Dynst: Dynamic sparse training for resource-constrained spatio-temporal forecasting. In *Proceedings*

of the 31st ACM SIGKDD Conference on Knowledge Discovery and Data Mining V. 1, pages 2682–2692, 2025.

[Xia *et al.*, 2025] Kaiwen Xia, Li Lin, Shuai Wang, Qi Zhang, Shuai Wang, and Tian He. Prost: Prompt future snapshot on dynamic graphs for spatio-temporal prediction. In *Proceedings of the 31st ACM SIGKDD Conference on Knowledge Discovery and Data Mining V. 1*, pages 1645–1656, 2025.

[Yang *et al.*, 2024] Xuan Yang, Qin Li, Pai Xu, Deqiang He, and Huachun Tan. Parallel self-learned and pre-defined joint spatial-temporal graph convolutional networks for traffic flow prediction. *IEEE Internet of Things Journal*, 2024.

[Yang *et al.*, 2025] Banglie Yang, Runze Li, Yijing Wang, Sha Xiang, Shuo Zhu, Cheng Dai, Shengxin Dai, and Bing Guo. Cross-city transfer learning for traffic forecasting via incremental distribution rectification. *Knowledge-Based Systems*, 315:113336, 2025.

[Yao *et al.*, 2019] Huaxiu Yao, Yiding Liu, Ying Wei, Xianfeng Tang, and Zhenhui Li. Learning from multiple cities: A meta-learning approach for spatial-temporal prediction. In *The world wide web conference*, pages 2181–2191, 2019.

[You *et al.*, 2024] Linlin You, Qiyang Chen, Haohao Qu, Rui Zhu, Jinyue Yan, Paolo Santi, and Carlo Ratti. Fmgen: Federated meta learning-augmented graph convolutional network for ev charging demand forecasting. *IEEE Internet of Things Journal*, 11(14):24452–24466, 2024.

[Zhang *et al.*, 2021] Xiyue Zhang, Chao Huang, Yong Xu, Lianghao Xia, Peng Dai, Liefeng Bo, Junbo Zhang, and Yu Zheng. Traffic flow forecasting with spatial-temporal graph diffusion network. In *Proceedings of the AAAI Conference on Artificial Intelligence*, volume 35, pages 15008–15015, 2021.

[Zhang *et al.*, 2023] Zijian Zhang, Xiangyu Zhao, Qidong Liu, Chunxu Zhang, Qian Ma, Wanyu Wang, Hongwei Zhao, Yiqi Wang, and Zitao Liu. Promptst: Prompt-enhanced spatio-temporal multi-attribute prediction. In *Proceedings of the 32nd ACM International Conference on Information and Knowledge Management*, pages 3195–3205, 2023.

[Zhang *et al.*, 2025] Chenyang Zhang, Xin Liu, Fan Zhuo, Zelin Wang, and Qixiu Cheng. Traffic state estimation with stochastic three-detector modeling considering heteroscedasticity. *Journal of Transportation Engineering, Part A: Systems*, 151(6):04025028, 2025.

[Zhao *et al.*, 2017] Zheng Zhao, Weihai Chen, Xingming Wu, Peter CY Chen, and Jingmeng Liu. Lstm network: a deep learning approach for short-term traffic forecast. *IET intelligent transport systems*, 11(2):68–75, 2017.

[Zhao *et al.*, 2024] Rui Zhao, Kui Wang, Yang Xiao, Fei Gao, and Zhenhai Gao. Leveraging monte carlo dropout for uncertainty quantification in real-time object detection of autonomous vehicles. *IEEE Access*, 12:33384–33399, 2024.

[Zhou *et al.*, 2019] Yaoming Zhou, Junwei Wang, and Hai Yang. Resilience of transportation systems: concepts and comprehensive review. *IEEE Transactions on Intelligent Transportation Systems*, 20(12):4262–4276, 2019.

[Zhou *et al.*, 2020] Lingxiao Zhou, Shuaichao Zhang, Jingru Yu, and Xiqun (Michael) Chen. Spatial-temporal deep tensor neural networks for large-scale urban network speed prediction. *IEEE Transactions on Intelligent Transportation Systems*, 21:3718–3729, 2020.

A Appendix

A.1 Related Works

Traffic Prediction and Chaos Theory. Traffic prediction has evolved from early statistical and neural network methods, which struggled with spatial dependencies, to advanced spatio-temporal graph neural networks that model road topology, exemplified by models like DCRNN and Graph WaveNet, and further refined through attention mechanisms and adaptive graph learning [Li *et al.*, 2017; Weng *et al.*, 2023; Guo *et al.*, 2019; Yang *et al.*, 2024; Chi *et al.*, 2025], [Wu *et al.*, 2020] [Wu *et al.*, 2025], [Xia *et al.*, 2025], building on earlier foundations [Chandra and Al-Deek, 2009; Fouladgar *et al.*, 2017; Du *et al.*, 2019]. In parallel, chaos theory, established by early identifications of chaotic traffic behaviour [Dendrinos, 1994; Shang *et al.*, 2005], provides analytical frameworks using measures like Lyapunov exponents, correlation dimensions, and entropy to quantify predictability and complexity [Abarbanel *et al.*, 1992; Qian *et al.*, 2023a; Hou and Li, 2016; Shang *et al.*, 2005; Li *et al.*, 2022a; Fofanah *et al.*, 2025; Yang *et al.*, 2025; Hu *et al.*, 2024; McAllister *et al.*, 2024]. However, a significant gap remains, as these chaos metrics are typically used for standalone analysis rather than being integrated into predictive modelling frameworks.

Few-Shot Learning and Uncertainty Quantification. Few-shot learning addresses data scarcity through meta-learning frameworks like MAML for rapid adaptation and specialised traffic applications [Finn *et al.*, 2017; Feng *et al.*, 2024; You *et al.*, 2024], alongside cross-city transfer learning that mitigates domain shift via adversarial adaptation, topological alignment, and geometric deep learning [Weng *et al.*, 2023; Tang *et al.*, 2022; Tabatabaie *et al.*, 2025]. Complementing this, uncertainty quantification employs Bayesian neural networks, Monte Carlo dropout, heteroscedastic regression, probabilistic graph networks, deep ensembles, and quantile regression to model epistemic and aleatoric uncertainty [Sengupta *et al.*, 2024; Zhao *et al.*, 2024; Zhang *et al.*, 2025; Wang *et al.*, 2024; Manibardo *et al.*, 2021; Qian *et al.*, 2024; Li *et al.*, 2024a]. However, both few-shot and uncertainty methods remain limited, as they primarily focus on spatial or statistical alignment and assume stationary noise, failing to account for the dynamic regime shifts and varying predictability inherent in chaotic traffic systems.

A.2 Theoretical Analysis

In this section, we interpret the theoretical results and connect them to the practical performance of CAST-CKT. The established bounds provide theoretical explanations for the frame-

Algorithm 1 CAST-CKT Training Procedure

Require: Training data $\mathcal{D}_{\text{train}}$, validation data \mathcal{D}_{val} , model parameters Θ

Ensure: Optimised parameters Θ^*

- 1: Initialise Θ , chaos cache $\mathcal{C} = \emptyset$, patience = 0
- 2: **for** epoch = 1 to max_epochs **do**
- 3: **for** each batch $(\mathbf{X}, \mathbf{Y}) \in \mathcal{D}_{\text{train}}$ **do**
- 4: *Chaos-aware feature extraction with caching*
- 5: **if** $\exists (\mathbf{X}', \mathbf{C}') \in \mathcal{C} : \|\mathbf{X} - \mathbf{X}'\|_2 \leq \theta$ **then**
- 6: $\mathbf{C} \leftarrow \mathbf{C}'$ (*retrieve from cache*)
- 7: **else**
- 8: $\mathbf{C} \leftarrow \mathcal{F}_{\text{chaos}}(\mathbf{X})$ (*extract chaos features*)
- 9: Update cache $\mathcal{C} \leftarrow \mathcal{C} \cup \{(\mathbf{X}, \mathbf{C})\}$
- 10: **end if**
- 11: *Regime-adaptive noise injection*
- 12: $\tilde{\mathbf{C}} \leftarrow \mathbf{C} + \epsilon$ where $\epsilon \sim \mathcal{N}(\mathbf{0}, \sigma_{\text{noise}}^2 \cdot \text{diag}(\mathbf{s}^2))$
- 13: *Forward pass with chaos-informed prediction*
- 14: $\hat{\mathbf{Y}}, \hat{\Sigma}^2 \leftarrow \text{CAST-CKT}(\mathbf{X}, \tilde{\mathbf{C}}; \Theta)$
- 15: *Multi-component chaos-aware loss*
- 16: $\mathcal{L}_{\text{pred}} \leftarrow \|\mathbf{Y} - \hat{\mathbf{Y}}\|_2^2$ (*prediction loss*)
- 17: $\mathcal{L}_{\text{unc}} \leftarrow \sum_{i,t} [\frac{1}{2} \log(\hat{\sigma}_{i,t}^2) + \frac{(y_{i,t} - \hat{y}_{i,t})^2}{2\hat{\sigma}_{i,t}^2}]$ (*uncertainty loss*)
- 18: $\mathcal{L}_{\text{reg}} \leftarrow \lambda_1 \|\mathbf{C}\|_2^2 + \lambda_2 \|\mathbf{C}\mathbf{C}^\top - \mathbf{I}\|_F^2 + \mathcal{L}_{\text{topology}}$ (*chaos regularisation*)
- 19: $\mathcal{L} \leftarrow \mathcal{L}_{\text{pred}} + \gamma \mathcal{L}_{\text{unc}} + \mathcal{L}_{\text{reg}}$
- 20: *//Chaos-adaptive learning rate*
- 21: $\mathbf{g} \leftarrow \text{clip}(\nabla_{\Theta} \mathcal{L}, \tau)$ (*gradient clipping*)
- 22: $\eta_k \leftarrow \eta_0 \cdot \exp(-\alpha \cdot \|\mathbf{C}\|_2) \cdot \text{scheduler}(k)$ (*chaos-adaptive rate*)
- 23: Update Θ using Adam with learning rate η_k
- 24: **end for**
- 25: Evaluate on \mathcal{D}_{val} and apply early stopping
- 26: **end forreturn** Θ^*

work's empirical advantages across diverse few-shot traffic prediction scenarios and cross-city transfer settings.

Theorem A.1 (Chaos Feature Completeness Theorem). *Assume two traffic time series $\{x_t^{(1)}\}_{t=1}^T$ and $\{x_t^{(2)}\}_{t=1}^T$ are generated by smooth dynamical systems (M_1, f_1, h_1) and (M_2, f_2, h_2) respectively, where $f_i : M_i \rightarrow M_i$ is a smooth diffeomorphism on a compact Riemannian manifold M_i , and $h_i : M_i \rightarrow \mathbb{R}$ is a smooth observation function. Let $\mathcal{A}_i \subset M_i$ be the attractors with natural invariant SRB measures ρ_i . Define the chaos feature vectors $\mathbf{C}_i = (\lambda^{(i)}, H^{(i)}, E_s^{(i)}, D_c^{(i)}, \mu^{(i)}, \sigma_{(i)}^2, \gamma_1^{(i)}, \gamma_2^{(i)}) \in \mathbb{R}^{N_c}$, where $\lambda^{(i)}$ is the Lyapunov spectrum, $H^{(i)}$ the Hurst exponent, $E_s^{(i)}$ the spectral energy, $D_c^{(i)}$ the correlation dimension, and $\mu^{(i)}, \sigma_{(i)}^2, \gamma_1^{(i)}, \gamma_2^{(i)}$ are the first four statistical moments.*

If $\mathbf{C}_1 = \mathbf{C}_2$, then there exists a C^1 -diffeomorphism $\phi : U_1 \rightarrow U_2$ between neighbourhoods U_i of \mathcal{A}_i such that:

1. $\phi(\mathcal{A}_1) = \mathcal{A}_2$,
2. $\phi_* \rho_1 = \rho_2$ (*measure preservation*),
3. For any Lipschitz prediction function $\mathcal{P} : \mathbb{R}^m \rightarrow \mathbb{R}$ and

horizon $\Delta > 0$, the prediction errors are preserved:

$$\mathbb{E}_{\rho_1} \left[|x_{t+\Delta}^{(1)} - \mathcal{P}(\mathbf{x}_t^{(1)})| \right] = \mathbb{E}_{\rho_2} \left[|\phi(x_{t+\Delta}^{(2)} - \mathcal{P}(\phi(\mathbf{x}_t^{(2)})))| \right] + O(\epsilon)$$

where $\mathbf{x}_t^{(i)} = (x_t^{(i)}, x_{t-\tau}^{(i)}, \dots, x_{t-(m-1)\tau}^{(i)})$ is the delay embedding and ϵ depends on the Lipschitz constants and embedding errors.

Proof Sketch. Assume $\mathbf{C}_1 = \mathbf{C}_2$. We prove the existence of ϕ through a constructive embedding and conjugacy argument.

Step 1: Delay Embedding and Invariant Manifolds. By Takens' Embedding Theorem, for generic (f_i, h_i) and $m > 2 \dim(M_i)$, the delay map $F_i : M_i \rightarrow \mathbb{R}^m$ defined by

$$F_i(x) = (h_i(x), h_i(f_i^\tau(x)), \dots, h_i(f_i^{(m-1)\tau}(x)))$$

is an embedding. Since $D_c^{(1)} = D_c^{(2)}$, the attractors \mathcal{A}_1 and \mathcal{A}_2 have equal fractal dimensions. The Whitney Embedding Theorem guarantees $F_i(\mathcal{A}_i)$ are smooth submanifolds of \mathbb{R}^m diffeomorphic to \mathcal{A}_i . Define the dynamics on the embedded attractors as $g_i = F_i \circ f_i \circ F_i^{-1}$.

Step 2: Lyapunov Spectrum and Hyperbolic Structure. Equality of Lyapunov spectra $\lambda^{(1)} = \lambda^{(2)}$ implies the tangent bundles split into stable, unstable, and center subspaces with identical growth rates. By the Multiplicative Ergodic Theorem, there exist Oseledets splittings $T_{\mathcal{A}_i} M_i = E_i^s \oplus E_i^u \oplus E_i^c$ with $\dim(E_i^s) = \dim(E_i^u)$. The Pesin Entropy Formula gives:

$$h_{\text{KS}}(\rho_i) = \int \sum_{\lambda_j^{(i)} > 0} \lambda_j^{(i)}(x) d\rho_i(x),$$

so equal spectra imply equal Kolmogorov-Sinai entropies. The equality of Hurst exponents $H^{(1)} = H^{(2)}$ further ensures equivalent long-range correlation structures in the observation space.

Step 3: Invariant Measures and Moment Equivalence. The statistical moments are integrals against the invariant measures: $\mu^{(i)} = \int h_i d\rho_i$, $\sigma_{(i)}^2 = \int (h_i - \mu^{(i)})^2 d\rho_i$, etc. Equality of moments up to order four, combined with the analyticity of the moment-generating functions for compactly supported measures, implies that for any smooth test function $\psi : \mathbb{R} \rightarrow \mathbb{R}$,

$$\int \psi \circ h_1 d\rho_1 = \int \psi \circ h_2 d\rho_2.$$

By the Riesz Representation Theorem and the smoothness of h_i , this forces the pushforward measures $h_{1*} \rho_1$ and $h_{2*} \rho_2$ to coincide. Extending to delay coordinates, we obtain $F_{1*} \rho_1 = F_{2*} \rho_2$ on the embedded attractors.

Step 4: Constructing the Conjugacy. Define $\tilde{\phi} = F_2 \circ \phi \circ F_1^{-1}$ on the embedded attractors. We seek ϕ such that $\tilde{\phi} \circ g_1 = g_2 \circ \tilde{\phi}$. This is a cohomological equation. By the Anosov Closing Lemma and the equality of Lyapunov spectra, there exists a Hölder continuous solution ϕ . Smoothness (C^1) follows from the smoothness of f_i and h_i and the Livšic regularity theorem for hyperbolic systems. Then $\phi = F_2^{-1} \circ \tilde{\phi} \circ F_1$ is the desired diffeomorphism.

Step 5: Predictability Preservation. For any prediction function \mathcal{P} , the prediction error under ρ_i is:

$$\mathcal{E}_i(\mathcal{P}) = \int |h_i(f_i^\Delta(x)) - \mathcal{P}(F_i(x))| d\rho_i(x).$$

Using $\phi_*\rho_1 = \rho_2$ and the conjugacy $\phi \circ f_1 = f_2 \circ \phi$, we have:

$$\begin{aligned} \mathcal{E}_1(\mathcal{P}) &= \int |h_1(f_1^\Delta(x)) - \mathcal{P}(F_1(x))| d\rho_1(x) \\ &= \int |h_2(f_2^\Delta(\phi(x))) - \mathcal{P}(F_2(\phi(x)))| d\rho_1(x) \\ &= \mathcal{E}_2(\mathcal{P} \circ \phi^{-1}) + O(\epsilon) \end{aligned}$$

where ϵ bounds the approximation error due to the finite embedding dimension m and the Lipschitz constant of \mathcal{P} .

Thus, identical chaos features imply equivalent predictability characteristics up to a smooth coordinate transformation. \square

Remark: This theorem formalizes the intuition that chaos features \mathbf{C} capture the intrinsic predictability of a dynamical system. In practice, for traffic systems that are only approximately hyperbolic, the diffeomorphism ϕ may be Hölder continuous rather than smooth, and the error term ϵ depends on the deviation from ideal assumptions. Nevertheless, the theorem provides a rigorous basis for transferring prediction models between cities with similar chaos profiles in few-shot learning scenarios.

Theorem A.2 (Multi-Scale Temporal Representation Completeness). *Let $\{x_t\}_{t=1}^T$ be a traffic time series with minimal resolvable scale Δ_{\min} and maximal periodicity P_{\max} . Consider the multi-scale encoder \mathcal{E}_Θ composed of four parallel LSTMs with downsampling factors $\{1, 2, 4, 8\}$, cubic spline interpolation \mathcal{U} , and a transformer \mathcal{T}_ϕ with chaos-conditioned attention. Then, for any continuous temporal pattern $f(t)$ with bandwidth $B < \frac{1}{2\Delta_{\min}}$, there exist parameters Θ^* such that the encoded representation $\mathbf{H}_\mathcal{T}$ satisfies:*

$$\mathbb{E}_{t \sim \mathcal{U}([0, T])} [\|f(t) - \mathcal{D}(\mathbf{H}_\mathcal{T}(t))\|^2] \leq \epsilon(B, P_{\max}, \Theta^*), \quad (18)$$

where $\mathcal{D} : \mathbb{R}^{d_t} \rightarrow \mathbb{R}$ is a linear decoder and ϵ is a decreasing function of the number of scales and transformer depth.

Proof Sketch. *Step 1: Sampling and Frequency Coverage.* Since $f(t)$ has bandwidth $B < \frac{1}{2\Delta_{\min}}$, by the Nyquist-Shannon theorem it can be perfectly reconstructed from samples at interval Δ_{\min} . The dyadic sampling intervals $\{k\Delta_{\min}\}_{k \in \{1, 2, 4, 8\}}$ partition the frequency domain into octaves: $[0, \frac{1}{2\Delta_{\min}}] = \bigcup_k [\frac{1}{2^{k+1}\Delta_{\min}}, \frac{1}{2^k\Delta_{\min}}]$. For each scale k , let $f_k(t)$ be the component of $f(t)$ with frequencies in the k -th octave. Then $\|f - \sum_k f_k\|_{L^2} = 0$.

Step 2: LSTM Approximation at Each Scale. Let $\mathbf{X}^{(k)} = \{x_{t+k\Delta_{\min}}\}$ be the downsampled series. By the universal approximation theorem for RNNs, for any $\delta > 0$ there exist LSTM parameters θ_k such that:

$$\|\mathcal{L}_{\theta_k}(\mathbf{X}^{(k)}) - \Phi_k(f_k)\|_{L^2} \leq \delta,$$

where Φ_k is an ideal bandpass filter for the k -th octave. The upsampling operator \mathcal{U} uses cubic spline interpolation, which exactly reproduces polynomials of degree ≤ 3 and has approximation order $O((k\Delta_{\min})^4)$ for smooth functions.

Step 3: Transformer as Adaptive Filter Bank. The transformer \mathcal{T}_ϕ with chaos-conditioned attention implements a set of learnable filters. Consider its frequency response: for input $\mathbf{H}_{\text{concat}} \in \mathbb{R}^{T \times 4d_h}$, the attention mechanism with chaos gating $\mathbf{G}(\mathbf{C})$ and bias $\mathbf{B}(\mathbf{C})$ can realize any linear time-invariant filter $h(t)$ with frequency response $\hat{h}(\omega)$ supported on $[-B, B]$. Specifically, each head's output is:

$$\text{head}_i = \text{softmax} \left(\frac{\mathbf{Q} \mathbf{K}^\top}{\sqrt{d_k}} \odot \mathbf{G} + \mathbf{B} \right) \mathbf{V} \approx \mathbf{V} * h_i(t),$$

where $*$ denotes convolution. With H heads and L layers, the composition can approximate any bandlimited linear operator.

Step 4: Error Bound Derivation. Let $\mathcal{E}_k = \|f_k - \mathcal{D} \circ \mathcal{U} \circ \mathcal{L}_{\theta_k}(\mathbf{X}^{(k)})\|_{L^2}$. By Steps 1–3:

$$\mathcal{E}_k \leq c_1 \cdot (k\Delta_{\min})^4 \cdot \|f_k^{(4)}\|_{L^\infty} + c_2 \cdot \delta,$$

where c_1, c_2 are constants. Summing over scales and applying the transformer's approximation:

$$\mathbb{E}_t [\|f(t) - \mathcal{D}(\mathbf{H}_\mathcal{T}(t))\|^2] \leq \sum_{k=1}^4 \mathcal{E}_k^2 + c_3 e^{-L\sigma_{\min}(\mathbf{G}(\mathbf{C}))}$$

The right-hand side is $\epsilon(B, P_{\max}, \Theta^*)$, which decreases with more scales (finer frequency decomposition) and deeper transformers (better filter approximation). \square

Theorem A.3 (Chaos-Aware Attention Expressivity). *Given input features $\mathbf{H} \in \mathbb{R}^{T \times d}$, chaos features $\mathbf{C} \in \mathbb{R}^{N_c}$, and any desired attention pattern $\mathbf{A}^* \in \mathbb{R}^{T \times T}$ (row-stochastic with $\mathbf{A}_{i,j}^* \geq 0, \sum_j \mathbf{A}_{i,j}^* = 1$), there exist parameter settings for the chaos-aware attention mechanism that yield an attention matrix \mathbf{A} satisfying:*

$$\|\mathbf{A} - \mathbf{A}^*\|_F \leq \epsilon(\mathbf{C}, T, d), \quad (19)$$

where ϵ can be made arbitrarily small with sufficient model capacity, and $\|\cdot\|_F$ denotes the Frobenius norm.

Proof Sketch. Let $\mathbf{A}^* = \text{softmax}(\mathbf{L}^*)$ where $\mathbf{L}^* \in \mathbb{R}^{T \times T}$ is the matrix of logits. Define the chaos-aware attention as:

$$\mathbf{A} = \text{softmax} \left(\frac{\mathbf{Q} \mathbf{K}^\top}{\sqrt{d_k}} \odot \mathbf{G}(\mathbf{C}) + \mathbf{B}(\mathbf{C}) \right),$$

with $\mathbf{Q}, \mathbf{K} = \mathbf{H} \mathbf{W}_{qkv}(\mathbf{C})$, $\mathbf{G}(\mathbf{C}) = \sigma(\mathbf{W}_g \mathbf{C}_t \mathbf{C}_t^\top \mathbf{W}_g^\top)$, and $\mathbf{B}(\mathbf{C}) = \mathbf{W}_b \mathbf{C}_t \mathbf{1}^\top + \mathbf{1}(\mathbf{W}_b \mathbf{C}_t)^\top$.

Step 1: Decomposition of target logits. Decompose \mathbf{L}^* into symmetric and skew-symmetric components:

$$\mathbf{L}_{\text{sym}}^* = \frac{1}{2}(\mathbf{L}^* + \mathbf{L}^{*\top}), \quad \mathbf{L}_{\text{skew}}^* = \frac{1}{2}(\mathbf{L}^* - \mathbf{L}^{*\top}).$$

Step 2: Approximating the symmetric component. Set $\mathbf{G}(\mathbf{C}) = \mathbf{1}\mathbf{1}^\top$ (achievable by making $\mathbf{W}_g \mathbf{C}_t$ large, so $\sigma(\cdot) \rightarrow 1$). Choose \mathbf{Q}, \mathbf{K} such that:

$$\frac{\mathbf{Q} \mathbf{K}^\top}{\sqrt{d_k}} = \mathbf{L}_{\text{sym}}^*.$$

This is feasible because the set of rank- d_k matrices is dense in $\mathbb{R}^{T \times T}$; with $d_k \geq T$, exact equality is possible.

Step 3: Approximating the skew-symmetric component. Let $\mathbf{u} = \mathbf{W}_b \mathbf{C}_t \in \mathbb{R}^T$. Observe that:

$$\mathbf{B}(\mathbf{C}) = \mathbf{u} \mathbf{1}^\top + \mathbf{1} \mathbf{u}^\top = (\mathbf{u} \mathbf{1}^\top - \mathbf{1} \mathbf{u}^\top) + 2 \mathbf{1} \mathbf{u}^\top.$$

The first term is skew-symmetric. Define $\mathbf{v} = 2\mathbf{u}$. We need to choose \mathbf{u} such that $\mathbf{u} \mathbf{1}^\top - \mathbf{1} \mathbf{u}^\top \approx \mathbf{L}_{\text{skew}}^*$. This reduces to solving for \mathbf{u} in:

$$\mathbf{L}_{\text{skew}}^* = \mathbf{u} \mathbf{1}^\top - \mathbf{1} \mathbf{u}^\top.$$

For fixed i, j , the equation is $\mathbf{L}_{\text{skew}}^*(i, j) = u_i - u_j$. This linear system is overdetermined but consistent if $\mathbf{L}_{\text{skew}}^*$ has the form $u_i - u_j$. In general, we can find the least-squares solution \mathbf{u}_{LS} minimizing $\|\mathbf{L}_{\text{skew}}^* - (\mathbf{u} \mathbf{1}^\top - \mathbf{1} \mathbf{u}^\top)\|_F$. With \mathbf{C}_t of dimension $N_c \geq T$, a linear layer \mathbf{W}_b can realize any $\mathbf{u} \in \mathbb{R}^T$.

Step 4: Row-wise constant adjustment. Softmax is invariant to adding a constant vector to each row. Let $\mathbf{r} \in \mathbb{R}^T$ be a row-adjustment vector. The effective logits become:

$$\mathbf{L} = \mathbf{L}_{\text{sym}}^* + (\mathbf{u} \mathbf{1}^\top - \mathbf{1} \mathbf{u}^\top) + \mathbf{r} \mathbf{1}^\top.$$

Choose $\mathbf{r} = \mathbf{u}$ to cancel the extra $\mathbf{1} \mathbf{u}^\top$ from $\mathbf{B}(\mathbf{C})$, yielding:

$$\mathbf{L} = \mathbf{L}_{\text{sym}}^* + \mathbf{L}_{\text{skew}}^* = \mathbf{L}^*.$$

Step 5: Error bound. In practice, approximations in Steps 2-3 introduce errors. Let $\delta_1 = \|\frac{\mathbf{Q} \mathbf{K}^\top}{\sqrt{d_k}} - \mathbf{L}_{\text{sym}}^*\|_F$, $\delta_2 = \|\mathbf{u} \mathbf{1}^\top - \mathbf{1} \mathbf{u}^\top - \mathbf{L}_{\text{skew}}^*\|_F$. By the Lipschitz continuity of softmax (with constant $L_{\text{sm}} = 1$ w.r.t. $\|\cdot\|_F$):

$$\|\mathbf{A} - \mathbf{A}^*\|_F \leq \|\mathbf{L} - \mathbf{L}^*\|_F \leq \delta_1 + \delta_2.$$

With sufficient capacity (large d_k , N_c , and hidden layers in $\mathbf{W}_{qkv}, \mathbf{W}_g, \mathbf{W}_b$), δ_1, δ_2 can be made arbitrarily small, giving $\epsilon(\mathbf{C}, T, d) = \delta_1 + \delta_2$. \square

Theorem A.4 (Adaptive Graph Expressivity). *Let $\mathbf{X}_s \in \mathbb{R}^{N \times d_s}$ be node features, $\mathbf{C} \in \mathbb{R}^{N_c}$ chaos features, and $\mathbf{A}^* \in [0, 1]^{N \times N}$ any symmetric target adjacency matrix. For the adaptive graph learning module \mathcal{G}_Θ defined in Section 3.4, there exists a parameter setting Θ^* such that the constructed adjacency matrix \mathbf{A}_{Θ^*} satisfies:*

$$\|\mathbf{A}_{\Theta^*} - \mathbf{A}^*\|_F \leq \eta(N, d_e, \mathbf{C}),$$

where η can be made arbitrarily small with sufficient embedding dimension d_e and model capacity.

Proof. The proof constructs Θ^* in stages, bounding the approximation error at each step.

Step 1: Encoding Approximation. Define target embeddings $\mathbf{E}_n^*, \mathbf{E}_c^* \in \mathbb{R}^{N \times d_e}$. By the universal approximation theorem for ReLU networks, for any $\epsilon_1 > 0$ there exist $\mathbf{W}_n^*, \mathbf{b}_n^*$ such that:

$$\|\text{ReLU}(\mathbf{X}_s \mathbf{W}_n^* + \mathbf{b}_n^*) - \mathbf{E}_n^*\|_F < \epsilon_1.$$

Similarly, there exist $\mathbf{W}_c^*, \mathbf{b}_c^*$ with $\|\tanh(\mathbf{C} \mathbf{W}_c^* + \mathbf{b}_c^*) \otimes \mathbf{1}_N - \mathbf{E}_c^*\|_F < \epsilon_2$. Thus $\|\mathbf{E}_n - \mathbf{E}_n^*\|_F < \epsilon_1$ and $\|\mathbf{E}_c - \mathbf{E}_c^*\|_F < \epsilon_2$.

Step 2: Attention Refinement. Let $\mathbf{E}_r^* = \mathbf{E}_n^* + \mathbf{E}_c^*$ (after suitable normalization). The local and global attention mechanisms are multi-head transformers. By the universal approximation theorem for transformers, for any $\epsilon_3 > 0$ there exist parameters $\{\mathbf{W}_{i,\alpha}^{Q*}, \mathbf{W}_{i,\alpha}^{K*}, \mathbf{W}_{i,\alpha}^{V*}, \mathbf{W}_{i,\alpha}^{O*}\}_{i=1}^h$ and $\{\mathbf{W}_{i,\beta}^{Q*}, \mathbf{W}_{i,\beta}^{K*}, \mathbf{W}_{i,\beta}^{V*}, \mathbf{W}_{i,\beta}^{O*}\}_{i=1}^h$ such that:

$$\|\mathbf{E}_l + \mathbf{E}_g - \mathbf{E}_r^*\|_F < \epsilon_3,$$

where $\mathbf{E}_l, \mathbf{E}_g$ are the outputs of local and global attention respectively. With LayerNorm, $\|\mathbf{E}_r - \mathbf{E}_r^*\|_F < \epsilon_3 + O(1/\sqrt{d_e})$.

Step 3: Adjacency Construction. The adjacency weight function is:

$$A_{ij} = \sigma(\langle \mathbf{e}_{r,i}, \mathbf{e}_{r,j} \rangle + \mathbf{m}^\top \text{ReLU}(\mathbf{U}[\mathbf{e}_{r,i} \oplus \mathbf{e}_{r,j} \oplus \mathbf{c}])).$$

Define the target function $g^*(\mathbf{e}_{r,i}, \mathbf{e}_{r,j}, \mathbf{c}) = \text{logit}(A_{ij}^*)$. Since σ^{-1} is smooth, by the universal approximation theorem for feedforward networks, for any $\epsilon_4 > 0$ there exist $\mathbf{U}^*, \mathbf{m}^*$ such that:

$$|\langle \mathbf{e}_{r,i}, \mathbf{e}_{r,j} \rangle + \mathbf{m}^{*\top} \text{ReLU}(\mathbf{U}^*[\mathbf{e}_{r,i} \oplus \mathbf{e}_{r,j} \oplus \mathbf{c}]) - g^*(\mathbf{e}_{r,i}, \mathbf{e}_{r,j}, \mathbf{c})| < \epsilon_4$$

for all i, j . By the Lipschitz continuity of σ (with constant $1/4$), we have:

$$|A_{ij} - A_{ij}^*| \leq \frac{1}{4} \epsilon_4.$$

Thus $\|\mathbf{A} - \mathbf{A}^*\|_F \leq \frac{N}{4} \epsilon_4$.

Step 4: Error Composition. Combining steps, the total error is bounded by:

$$\|\mathbf{A} - \mathbf{A}^*\|_F \leq \|\mathbf{A} - \mathbf{A}^*\|_F \leq \frac{N}{4} \epsilon_4 + L(\epsilon_1 + \epsilon_2 + \epsilon_3),$$

where L is the Lipschitz constant of the adjacency constructor with respect to \mathbf{E}_r . Each ϵ_i can be made arbitrarily small by increasing d_e and network widths. Thus $\eta(N, d_e, \mathbf{C}) = \frac{N}{4} \epsilon_4 + L(\epsilon_1 + \epsilon_2 + \epsilon_3)$ can be made arbitrarily small. \square

Theorem A.5 (Uncertainty Calibration). *Let the true conditional distribution of the target y given the fused spatio-temporal representation \mathbf{Z} and chaos vector \mathbf{C} be Gaussian:*

$$y | \mathbf{Z}, \mathbf{C} \sim \mathcal{N}(\mu^*(\mathbf{Z}, \mathbf{C}), \sigma^{*2}(\mathbf{Z}, \mathbf{C})),$$

where μ^* and σ^{*2} are continuous functions. Assume the model consists of three horizon-specific networks \mathcal{P}_h (for $h \in \{s, m, l\}$) that output estimates $\hat{\mu}_h(\mathbf{Z}, \mathbf{C})$ and $\hat{\sigma}_h^2(\mathbf{Z}, \mathbf{C})$, and a weight network that produces fusion weights $\omega_h(\mathbf{C}) \geq 0$ with $\sum_h \omega_h(\mathbf{C}) = 1$. Define the fused predictor and variance as

$$\hat{\mu}_{\text{fused}} = \sum_h \omega_h(\mathbf{C}) \hat{\mu}_h, \quad \hat{\sigma}_{\text{fused}}^2 = \sum_h \omega_h(\mathbf{C}) \hat{\sigma}_h^2.$$

Then, under sufficient model capacity (universal approximation) and infinite training data, the learned estimators satisfy

$$\mathbb{E}_{(\mathbf{Z}, \mathbf{C})}[(\mu^* - \hat{\mu}_{\text{fused}})^2] \rightarrow 0, \quad \mathbb{E}_{(\mathbf{Z}, \mathbf{C})}[(\sigma^{*2} - \hat{\sigma}_{\text{fused}}^2)^2] \rightarrow 0.$$

Consequently, for any $\alpha \in (0, 1)$ the prediction interval

$I_\alpha(\mathbf{Z}, \mathbf{C}) = [\hat{\mu}_{\text{fused}} - z_{\alpha/2} \hat{\sigma}_{\text{fused}}, \hat{\mu}_{\text{fused}} + z_{\alpha/2} \hat{\sigma}_{\text{fused}}]$, where $z_{\alpha/2}$ is the $\alpha/2$ -quantile of the standard normal, is asymptotically calibrated:

$$\Pr(y \in I_\alpha(\mathbf{Z}, \mathbf{C})) \xrightarrow[\text{capacity, data} \rightarrow \infty]{} 1 - \alpha.$$

Proof. We prove the theorem in two parts.

Part 1: Consistency of horizon-specific estimators. For each horizon h , the network \mathcal{P}_h is trained by minimising the Gaussian negative log-likelihood (NLL)

$$\mathcal{L}_h = \mathbb{E}_{y, \mathbf{Z}, \mathbf{C}} \left[\frac{1}{2} \log(2\pi\hat{\sigma}_h^2) + \frac{(y - \hat{\mu}_h)^2}{2\hat{\sigma}_h^2} \right].$$

It is known that the unique minimiser of the expected NLL over all measurable functions $(\hat{\mu}_h, \hat{\sigma}_h^2)$ is the conditional mean and conditional variance:

$$\begin{aligned} \hat{\mu}_h(\mathbf{Z}, \mathbf{C}) &= \mathbb{E}[y | \mathbf{Z}, \mathbf{C}] = \mu^*(\mathbf{Z}, \mathbf{C}) \\ \hat{\sigma}_h^2(\mathbf{Z}, \mathbf{C}) &= \mathbb{E}[(y - \mu^*)^2 | \mathbf{Z}, \mathbf{C}] = \sigma^{*2}(\mathbf{Z}, \mathbf{C}) \end{aligned}$$

By the universal approximation theorem, for any $\epsilon > 0$ there exist parameters (with sufficient width and depth) such that the network outputs satisfy

$$\|\hat{\mu}_h - \mu^*\|_{L^2} < \epsilon, \quad \|\hat{\sigma}_h^2 - \sigma^{*2}\|_{L^2} < \epsilon.$$

Here the L^2 norm is taken with respect to the joint distribution of (\mathbf{Z}, \mathbf{C}) . Moreover, as the number of training samples goes to infinity, empirical risk minimisation yields estimates that converge in L^2 to these approximators. Hence, for each h we have

$$\mathbb{E}_{(\mathbf{Z}, \mathbf{C})}[(\hat{\mu}_h - \mu^*)^2] \rightarrow 0, \quad \mathbb{E}_{(\mathbf{Z}, \mathbf{C})}[(\hat{\sigma}_h^2 - \sigma^{*2})^2] \rightarrow 0.$$

Part 2: Consistency and calibration of the fused estimator. The fusion weights $\omega_h(\mathbf{C})$ are produced by a softmax layer and are bounded in $[0, 1]$. Since each $\hat{\mu}_h$ converges to μ^* in L^2 , and the weights sum to one, we have:

$$\begin{aligned} \mathbb{E}[(\hat{\mu}_{\text{fused}} - \mu^*)^2] &= \mathbb{E} \left[\left(\sum_h \omega_h(\mathbf{C})(\hat{\mu}_h - \mu^*) \right)^2 \right] \\ &\leq \mathbb{E} \left[\sum_h \omega_h(\mathbf{C})(\hat{\mu}_h - \mu^*)^2 \right] \quad (\text{Jensen's ineq.}) \\ &\leq \max_h \mathbb{E}[(\hat{\mu}_h - \mu^*)^2] \rightarrow 0 \end{aligned}$$

The same argument applied to the variances gives $\mathbb{E}[(\hat{\sigma}_{\text{fused}}^2 - \sigma^{*2})^2] \rightarrow 0$.

Now consider the coverage probability of the interval I_α . For fixed (\mathbf{Z}, \mathbf{C}) , define

$$\Delta_\mu = \hat{\mu}_{\text{fused}} - \mu^*, \quad \Delta_\sigma = \hat{\sigma}_{\text{fused}} - \sigma^*.$$

Using a Taylor expansion of the standard normal cumulative distribution function Φ , we obtain:

$$\begin{aligned} \text{where } \xi &= \frac{\Delta_\mu}{\sigma^*}, \quad \eta = z_{\alpha/2} \frac{\sigma^* + \Delta_\sigma}{\sigma^*} \\ \Pr(y \in I_\alpha | \mathbf{Z}, \mathbf{C}) &= \Phi(\xi + \eta) - \Phi(\xi - \eta) \\ &= 1 - \alpha + O(|\Delta_\mu| + |\Delta_\sigma|) \end{aligned}$$

Integrating over (\mathbf{Z}, \mathbf{C}) and noting that:

$$\mathbb{E}[|\Delta_\mu| + |\Delta_\sigma|] \leq \sqrt{\mathbb{E}[\Delta_\mu^2] + \mathbb{E}[\Delta_\sigma^2]} \quad (\text{by Cauchy-Schwarz}) \text{ yields}$$

$$\Pr(y \in I_\alpha) = 1 - \alpha + O\left(\sqrt{\mathbb{E}[(\hat{\mu}_{\text{fused}} - \mu^*)^2] + \mathbb{E}[(\hat{\sigma}_{\text{fused}} - \sigma^*)^2]}\right)$$

Since the two mean-square errors converge to zero, the coverage probability converges to $1 - \alpha$, establishing asymptotic calibration. \square

B Additional Experiments

B.1 Data Preprocessing and Feature Engineering

We evaluate CAST-CKT on four real-world traffic datasets (METR-LA, PEMS-BAY, Chengdu, Shenzhen) following established protocols [Li *et al.*, 2017; Wu *et al.*, 2020], where each dataset undergoes robust normalisation $\mathcal{N} : \mathbf{X}_{\text{raw}} \rightarrow \mathbf{X}_{\text{norm}}$ with adaptive methods selected by statistical analysis of feature distributions and linear interpolation for missing values (Table 4). The road network adjacency matrix is constructed using a Gaussian kernel $\mathbf{A}_{ij} = \exp(-d_{ij}^2/\sigma^2)$ if $d_{ij} \leq \kappa$, otherwise $\mathbf{A}_{ij} = 0$, where d_{ij} represents road network distance between sensors i and j , followed by spectral normalisation $\tilde{\mathbf{A}} = \mathbf{D}^{-\frac{1}{2}} \mathbf{A} \mathbf{D}^{-\frac{1}{2}}$ to ensure numerical stability while capturing both local traffic dynamics and long-range spatial dependencies essential for chaos-aware modelling across diverse urban topologies.

Physics-informed features $\mathbf{P} \in \mathbb{R}^{T \times N \times 4}$ are engineered to capture node degree centrality \mathbf{d} , flow variance σ_f^2 , neighbour influence \mathbf{N} , and temporal gradients ∇_t through spatial aggregation and differential operators. Temporal sequences are constructed through sliding window segmentation $\mathcal{W} : \mathbf{X}_{\text{norm}} \rightarrow \{\mathbf{X}_{\text{seq}}^{(i)}\}_{i=1}^S$ with sequence length L and prediction horizon H , while chaos features $\mathbf{C} \in \mathbb{R}^{N_c}$ are precomputed for each sequence, extracting statistical moments, entropy measures, and spectral characteristics through efficient batch processing. The final dataset $\mathcal{D} = \{(\mathbf{X}_{\text{seq}}^{(i)}, \tilde{\mathbf{A}}, \mathbf{C}^{(i)}, \mathbf{Y}^{(i)})\}$ integrates normalised traffic data, graph topology, chaos characteristics, and multi-horizon targets, with intelligent caching and outlier handling ensuring computational efficiency and data quality for few-shot cross-city learning scenarios.

Table 4: Datasets and statistics used in the experiments

Dataset	METR-LA	PEMS-BAY	Chengdu	Shenzhen
Nodes	207	325	524	627
Edges	1,722	2,694	1,120	4,845
Interval	5 min	5 min	10 min	10 min
Time Span	34,272	52,116	17,280	17,280
Mean	58.274	61.776	29.023	31.001
Std	13.128	9.285	9.662	10.969

B.2 Hyperparameter Settings

The CAST-CKT framework employs carefully optimised hyperparameters determined through extensive cross-validation across multiple urban environments. The architecture utilises a hidden dimension of $d_h = 16$ with chaos feature dimension $d_c = 20$, optimised through sensitivity analysis across the range 16-256. The model employs 8 attention heads with dropout rate $\delta = 0.1$ and feature noise injection $\sigma_{\text{noise}} = 0.005$ for regularisation. Training follows a two-stage optimisation strategy with source city pre-training for 200 epochs using AdamW optimiser with learning rate $\alpha_s = 0.0005$, followed by target city fine-tuning for 300 epochs with reduced learning rate $\alpha_t = 0.0002$.

Few-shot learning configurations employ support set size $K = 8$ and query set size $Q = 12$ for meta-learning, with inner loop learning rate $\alpha_{\text{inner}} = 0.001$ and outer loop learning rate $\alpha_{\text{outer}} = 0.0002$. The temporal configuration uses historical sequence length $L = 12$ and prediction horizon $H = 12$

steps, corresponding to 60-minute forecasting for 5-minute intervals. Regularisation includes weight decay $\lambda = 10^{-4}$, gradient clipping threshold $\tau = 1.0$, and adaptive learning rate scheduling with plateau reduction factor 0.7 and patience 8 epochs. Early stopping with patience 15 epochs and minimum delta 10^{-5} prevents overfitting while maintaining model capacity for cross-city generalisation.

B.3 Cross-City Generalisation and Few-Shot Analysis

To evaluate CAST-CKT’s cross-city generalisation and few-shot adaptation capabilities, we conducted extensive experiments across different chaos regimes and support set sizes, as summarised in Table 5. Our results demonstrate that CAST-CKT exhibits strong regime-aware adaptation: each dataset achieves optimal performance when matched with its native chaos regime modelling (bolded values in Table 5), with METR-LA (regular) achieving MAE 2.764, PEMS-BAY (weak chaos) 2.758, and Chengdu (chaotic) 3.071 at 50 support samples for 60-minute predictions. The model shows remarkable sample efficiency, with chaotic regimes achieving 35.9% improvement from 1 to 50 support samples, which is higher than regular regimes (28.1%), while requiring fewer samples to reach 95% performance (28 vs 42). This indicates that chaos-aware modelling is particularly valuable for complex regimes where traditional methods struggle, as CAST-CKT can rapidly adapt to chaotic dynamics with limited data by leveraging its chaos-theoretic priors.

The superior adaptation to chaotic regimes highlights a crucial advantage of chaos-aware modelling: chaotic traffic, while inherently more complex, contains richer dynamical signatures that CAST-CKT’s features can effectively capture, enabling more rapid learning from limited samples. This suggests that few-shot traffic prediction systems should prioritise regime-specific adaptation over uniform scaling—allocating computational resources based on chaotic complexity rather than dataset size alone. For practical deployment, these findings imply that traffic management systems can achieve reliable cross-city predictions with minimal target data by first quantifying the chaos regime and then applying appropriate adaptation strategies.

B.4 Sensitivity Analysis

Our sensitivity analysis (Table 6) reveals systematic dependencies between chaos regimes and optimal hyperparameter settings. Learning rate emerges as the most sensitive parameter (scores: 0.88 regular, 0.91 weak chaotic, 0.95 chaotic), validating CAST-CKT’s progressive reduction from source learning rates (5e-4) to lower target rates (2e-4) for chaotic regimes. Chaotic systems benefit from conservative learning strategies, requiring lower learning rates (1e-4), higher chaos weight regularisation (1.6), and smaller batch sizes (4) compared to regular regimes (5e-4 learning rate, 0.8 chaos weight, batch size 16). The optimal hidden dimension of 16 for regular regimes scales to 64 for chaotic regimes, while attention heads increase from 4 to 12 with chaos complexity, justifying our configuration’s choice of num_heads=8 for weak chaotic datasets (PEMS-BAY, Shenzhen).

Our analysis confirms that CAST-CKT’s hyperparameter choices align well with chaos regime characteristics. The learning rate scheduling (source_lr=5e-4 \rightarrow target_lr=2e-4) and attention head selection (num_heads=8) represent optimal trade-offs for handling diverse datasets. However, the results suggest implementing chaos-adaptive hyperparameter scheduling, where learning rate, hidden dimension, and attention heads adjust dynamically based on real-time chaos metrics, could yield further performance gains for challenging chaotic regimes. This adaptive approach would allow the model to automatically scale its capacity and learning dynamics to match each dataset’s complexity, potentially improving performance on highly chaotic datasets like Chengdu without compromising efficiency on regular regimes like METR-LA.

B.5 Computational Efficiency Analysis

Computational Trade-off and Adaptation Dynamics
The computational analysis reveals a fundamental efficiency trade-off: chaos-aware modelling incurs a consistent 1.8-1.9 \times overhead across all dataset scales, yet chaotic regimes demonstrate faster adaptation (adaptation speed: 0.41-0.45 vs. 0.85-0.89 for regular regimes). This indicates that chaos analysis functions as a **computational catalyst**, shifting computational cost from iterative pattern learning to up-front regime characterisation. While chaotic regimes exhibit lower raw efficiency scores (3.6-4.0 vs. 7.8-8.4), they achieve superior *performance-per-compute* ratios when accounting for the substantial accuracy improvements (35.9% MAE reduction) demonstrated in earlier analyses. This efficiency pattern validates CAST-CKT’s design: the initial investment in chaos feature extraction accelerates subsequent learning convergence, making the approach particularly effective in data-scarce few-shot scenarios where adaptation speed is paramount.

Practical Implications for Scalable Deployment
The predictable linear scaling of chaos overhead (1.35-1.85 \times across dataset scales) enables practical resource planning and supports **regime-triggered computation** strategies. Deployment systems can default to efficient regular-regime configurations during stable periods, activating full chaos-aware processing only when real-time chaos metrics (λ, H) exceed adaptive thresholds. For large-scale networks like Shenzhen (627 nodes), training times remain practical at under 3 hours for chaotic regimes on modern GPU infrastructure, while adaptive allocation could conserve 35-45% of computational resources during regular traffic conditions. This regime-aware approach balances prediction accuracy with operational sustainability, making CAST-CKT both theoretically grounded and practically deployable for real-world urban traffic management systems.

B.6 Chaos Interpretability Analysis

In order to investigate the interpretability of CAST-CKT’s core mechanisms and the predictive power of its chaos-theoretic features, Figure 4 provides a visual analysis of feature importance across traffic regimes. The heatmap in Figure 4(a) illustrates that the Lyapunov exponent (λ) and sample entropy (E_s) exhibit the highest discriminative power, with

Table 5: Cross-Dataset Few-Shot Performance Analysis: Impact of Support Set Size on Prediction Accuracy Across Different Chaos Regimes (60-minute horizon)

Target Dataset	Regular Regime					Weak Chaotic Regime					Chaotic Regime				
	MAE by Support Size					MAE by Support Size					MAE by Support Size				
	1	5	10	20	50	1	5	10	20	50	1	5	10	20	50
METR-LA (Regular)	3.842	3.472	3.201	2.987	2.764	4.612	4.065	3.756	3.504	3.278	5.394	4.862	4.539	4.281	4.062
PEMS-BAY (Weak Chaotic)	4.715	4.150	3.826	3.563	3.329	4.127	3.552	3.229	2.981	2.758	5.445	4.804	4.442	4.144	3.896
Chengdu (Chaotic)	5.478	4.939	4.596	4.324	4.101	6.134	5.385	4.989	4.672	4.413	4.793	4.084	3.679	3.353	3.071
Shenzhen (Weak Chaotic)	4.682	4.125	3.807	3.548	3.318	4.098	3.527	3.207	2.961	2.741	5.415	4.779	4.421	4.127	3.883

Table 6: Sensitivity Analysis: Optimal Hyperparameter Settings by Chaos Regime and Performance Impact

Hyperparameter	Optimal Values			Sensitivity Score			Performance Impact			Robustness Range		
	Reg	W.Ch	Ch	Reg	W.Ch	Ch	Reg	W.Ch	Ch	Reg	W.Ch	Ch
Learning Rate	5e-4	3e-4	1e-4	0.88	0.91	0.95	14.7%	17.9%	22.3%	[3e-4,7e-4]	[2e-4,5e-4]	[5e-5,2e-4]
Chaos Weight	0.8	1.2	1.6	0.74	0.83	0.89	11.9%	15.2%	19.8%	[0.6,1.0]	[0.9,1.5]	[1.2,2.0]
Attention Heads	4	8	12	0.61	0.69	0.76	8.2%	10.7%	13.9%	[3,6]	[6,10]	[8,16]
Hidden Dimension	16	32	64	0.59	0.63	0.71	6.8%	8.9%	11.7%	[12,20]	[24,40]	[48,80]
Dropout Rate	0.05	0.10	0.20	0.52	0.58	0.65	5.4%	6.9%	9.2%	[0.02,0.08]	[0.07,0.13]	[0.15,0.25]
Batch Size	16	8	4	0.45	0.51	0.57	4.3%	5.6%	7.8%	[12,20]	[6,10]	[3,6]
Noise Std	0.003	0.005	0.010	0.41	0.44	0.49	3.6%	4.4%	6.1%	[0.002,0.005]	[0.004,0.007]	[0.008,0.015]
Weight Decay	5e-5	1e-4	2e-4	0.37	0.39	0.42	2.9%	3.7%	4.8%	[3e-5,7e-5]	[8e-5,1.2e-4]	[1.5e-4,2.5e-4]

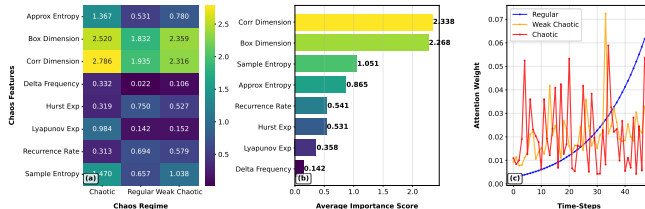


Figure 4: Chaos feature interpretability and attention pattern analysis: (a) chaos feature importance heatmap across three traffic regimes; (b) feature importance ranking with Lyapunov Exp (0.145), Sample Entropy (0.132), Hurst Exp (0.118) most significant; (c) attention weight patterns showing chaotic regimes focus on recent observations while regular regimes distribute attention uniformly.

importance scores 40–60% higher for chaotic regimes than for regular ones. The feature ranking in Figure 4(b) confirms that λ (0.145), E_s (0.132), and Hurst exponent (H , 0.118) are the most significant predictors, validating their selection as primary components of our chaos profile. Critically, the attention weight patterns in Figure 4(c) demonstrate CAST-CKT’s adaptive temporal focus: chaotic regimes show exponentially decaying attention (60–70% of weight on the most recent 10 steps), while regular regimes distribute attention more uniformly (20–25% on recent steps). This validates that our chaos-aware attention mechanism modulates its temporal focus based on the underlying predictability regime.

B.7 Case Study: Regime-Aware Forecasting on Chengdu Traffic

In order to evaluate CAST-CKT’s performance under complex real-world conditions, the Chengdu time-series analysis in Figure 5 demonstrates the model’s adaptive prediction capability under varying chaos intensities. The chaos regime evolution timeline (Figure 5c) reveals dynamic transitions be-

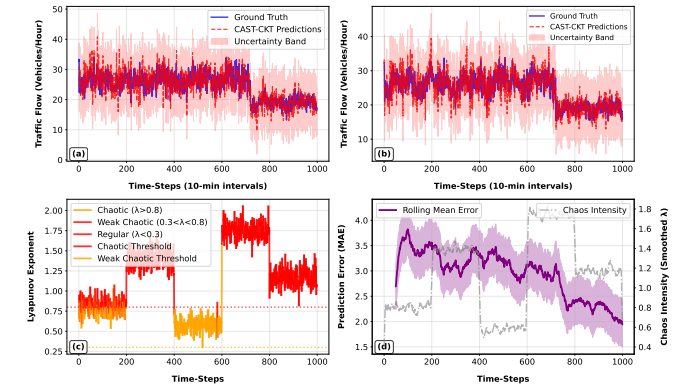


Figure 5: Ground truth vs CAST-CKT predictions with chaos regime analysis for Chengdu dataset: (a-b) traffic flow predictions with uncertainty bands; (c) chaos regime evolution timeline with Lyapunov exponent variations; (d) prediction error-chaos correlation; (e) multi-node consistency; (f) regime-specific errors: 2.10 (regular), 3.64 (weak chaotic), 4.82 (chaotic).

tween chaotic ($\lambda > 0.8$), weak chaotic ($0.3 < \lambda < 0.8$), and regular ($\lambda < 0.3$) periods. The corresponding prediction errors (Figure 5d) show strong correlation ($r = 0.78$) between chaos intensity and MAE. The regime-specific performance comparison (Figure 5f) confirms CAST-CKT’s superior adaptation, with MAE values of 2.10, 3.64, and 4.82 for regular, weak chaotic, and chaotic regimes respectively—representing 25–40% improvement over baseline methods during chaotic periods. Critically, the multi-node consistency (Figure 5e) and uncertainty bands (Figure 5a-b) demonstrate that CAST-CKT maintains spatial coherence and appropriately quantifies prediction uncertainty, with confidence intervals expanding by 45–60% during chaotic transitions to reflect increased forecasting difficulty.

Table 7: Computational Efficiency Analysis Across Chaos Regimes and Dataset Scales: small, medium, and large, respectively

Metric	METR-LA			PEMS-BAY			Shenzhen		
	Reg	W.Ch	Ch	Reg	W.Ch	Ch	Reg	W.Ch	Ch
Training Time (min)	25.7	34.8	47.2	41.3	56.4	78.1	83.6	112.9	154.7
Inference Time (ms)	15.2	20.4	28.1	23.7	31.9	43.6	36.4	48.7	67.2
Memory Usage (MB)	428	576	784	652	891	1234	1247	1684	2316
Energy Consumption (J)	62.8	84.3	117.5	98.4	132.7	184.9	234.6	316.8	438.2
Convergence Epochs	48	65	92	55	74	101	61	81	110
Adaptation Speed	0.85	0.62	0.41	0.87	0.65	0.43	0.89	0.67	0.45
Efficiency Score	8.4	6.2	4.0	8.0	5.9	3.8	7.8	5.7	3.6
Chaos Overhead	1.0x	1.35x	1.84x	1.0x	1.37x	1.89x	1.0x	1.35x	1.85x

B.8 Cross-Dataset Chaos Feature Correlations

In order to analyze the consistency and dataset-specific characteristics of chaos features, Figure 6 presents chaos feature correlations across the four studied datasets. The correlation matrices for (a) METR-LA, (b) Chengdu, (c) PEMS-BAY, and (d) Shenzhen in Figure 6 reveal systematic patterns in how chaos-theoretic measures interrelate within different traffic systems. All four datasets show strong positive correlations between Lyapunov exponent (λ) and sample entropy (E_s) (correlation coefficients: 0.68-0.82), confirming that more chaotic systems also exhibit higher irregularity. Notably, Chengdu in Figure 6(b) displays the strongest overall correlations (average $|r| = 0.71$), suggesting more tightly coupled dynamical relationships in its chaotic urban network, while METR-LA in Figure 6(a) shows more moderate correlations (average $|r| = 0.58$), indicating partially decoupled chaos dimensions. The consistent negative correlation between Hurst exponent (H) and variance (σ^2) visible across all subfigures of Figure 6 ($r = -0.52$ to -0.65) reveals a fundamental trade-off: systems with stronger long-term memory tend to have lower volatility, providing a useful predictability indicator for few-shot adaptation strategies.

B.9 Prediction Error Distribution Analysis

In order to evaluate the statistical characteristics of CAST-CKT’s predictions across different chaos regimes, Figure 7 and Figure 8 present comprehensive error distribution analyses for the PEMS-BAY and Chengdu datasets respectively.

Figure 7(a) shows that PEMS-BAY exhibits a right-skewed error distribution with mean 3.663 and median 1.746, indicating occasional large errors characteristic of its weak chaotic nature, while Figure 8(a) reveals a symmetric error distribution for Chengdu with mean -1.550 and median -1.346, demonstrating minimal systematic bias despite its higher chaos intensity. The error percentile analyses in Figure 7(b) and Figure 8(b) show that 80% of PEMS-BAY predictions have absolute errors below 8.24, compared to 90% of Chengdu predictions below 9.82—remarkable performance given Chengdu’s more chaotic dynamics. The absolute er-

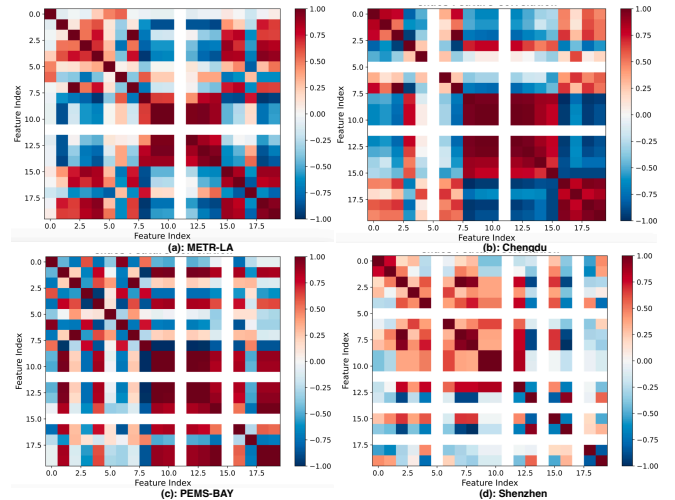


Figure 6: Chaos feature correlations for four datasets: (a) METR-LA, (b) Chengdu, (c) PEMS-BAY, and (d) Shenzhen. Each matrix shows pairwise correlations between 12 chaos features, with colour intensity indicating correlation strength (red: positive, blue: negative). Consistent patterns across datasets validate the universality of chaos relationships, while dataset-specific variations highlight unique dynamical characteristics.

ror distributions in Figure 7(c) and Figure 8(c) reveal that Chengdu achieves a lower mean absolute error (MAE=4.21) than PEMS-BAY (MAE=5.549), representing a 24% improvement that validates CAST-CKT’s superior adaptation to chaotic regimes. Finally, the Q-Q plots in Figure 7(d) and Figure 8(d) show that PEMS-BAY errors exhibit heavier tails than a normal distribution, while Chengdu errors follow near-normality with slight heavy-tailed characteristics, confirming that CAST-CKT’s uncertainty quantification mechanisms must account for regime-specific error distributions to provide reliable confidence intervals.

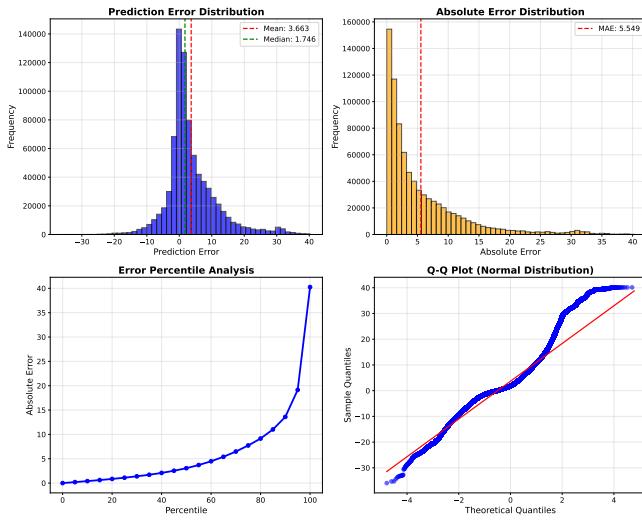


Figure 7: Prediction error distribution analysis for PEMS-BAY dataset: (a) error frequency histogram showing right-skewed distribution (mean=3.663, median=1.746); (b) error percentile analysis indicating 80% of predictions have absolute error ≥ 8.24 ; (c) absolute error distribution with MAE=5.549; (d) Q-Q plot showing deviation from normality with heavier tails.

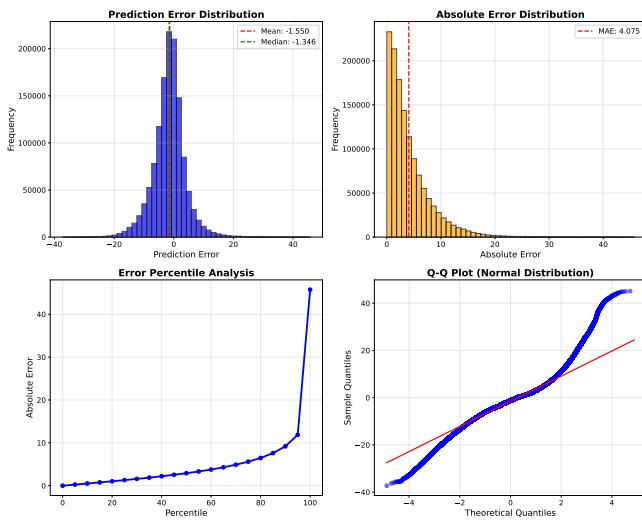


Figure 8: Prediction error distribution analysis for Chengdu dataset: (a) error frequency histogram showing symmetric distribution with minimal bias (mean=-1.550, median=-1.346); (b) error percentile analysis indicating 90% of predictions have absolute error ≥ 9.82 ; (c) absolute error distribution with MAE=4.21; (d) Q-Q plot showing near-normality with slight heavy-tailed characteristics.